A Novel Process to Create Arbitrary Microcellular Patterns in Polycarbonate using a Laser Beam

Rohil Anil Manakad

A thesis

submitted in partial fulfillment of the

requirements for the degree of

Master of Science in Mechanical Engineering

University of Washington

2021

Committee:

Vipin Kumar

Mohammad H. Malakooti

John Weller

Program Authorized to Offer Degree:

Mechanical Engineering

University of Washington

Abstract

A Novel Process to Create Arbitrary Microcellular Patterns in Polycarbonate using a Laser Beam

Rohil Anil Manakad

Chair of the Supervisory Committee:
Vipin Kumar
Department of Mechanical Engineering
Co-Chair of the Supervisory Committee:
Mohammad H. Malakooti
Department of Mechanical Engineering

Microcellular and nanocellular polymer foams offer a wide range of applications from food safety to aerospace industries. In this work, we introduce a versatile process to nucleate microcells in polycarbonate sheets via laser beam. This method allows local heating of CO_2 saturated polycarbonates which results in the creation of arbitrary shapes of microcellular foamed regions in a plastic part. We present the processing parameters required to create foams in polycarbonate sheets that were saturated with carbon dioxide at pressures of 1, 3 and 5 MPa. The relationship between the processing (input) factors of speed, power (of the laser beam), and the saturation pressure and the consequent microstructure produced (parameters like average cell size, foam depth, and melted surface thickness) is investigated. Energy delivered by the laser and the temperature rise at the surface of the specimen is also approximated. The feasibility of this process is also demonstrated on PEI. High resolution patterns of microcellular foams were directly written by a laser beam which shows the extraordinary level of control offered by this methodology. Intricate 2D digital designs are also produced using this novel approach.

Table of Contents

List of Figures ii

List of Tables iv

Chapter 1.0 Introduction 1

Chapter 2.0 Process Space Exploration 3

2.1 Procedure and Experiments Performed 3

2.2 Experimental catalog of foaming experiments at 1, 3 and 5 MPa: 4

2.3 Discussion of experimental results at different pressures: 19

2.4 Process Window Plots at 1, 3 and 5 MPa CO_2 saturation pressures 20

Chapter 3.0 Foam Microstructure 24

3.0.1 Observations from SEM micrographs 30

3.1 Average cell size measurement method using ImageJ 30

3.1.1 Limitations of this process 31

3.2 Variation of structure (average cell size) with speed at 5 MPa 32

Observations: 33

3.3 Variation of structure (average cell size) with power at 3 MPa 34

Observations: 35

Chapter 4.0 Energy and Temperature Considerations 36

4.1 Energy delivered to the specimen by the laser beam 36

4.2 Surface Temperature estimation of specimens 37

4.2.1 Model 1 – Considering Energy per dot 37

4.2.2 **Model 2 – Considering Total Energy delivered to the specimen and heat transfer losses** 38

Chapter 5.0 Conclusions and Recommendations 40

5.1 Conclusions 40

5.2 Recommendations for future work 41

5.2.1 Near-term ideas 41

5.2.2 Longer term research ideas 41

Chapter 6.0 References 45

Appendix 46

Additional foamed micrographs at 5 MPa: 46

Additional foamed micrographs at 3 MPa: 53

Additional foamed micrographs at 1 MPa: 60

List of Figures

Figure 1: Process Schematics 2
Figure 2a: Focusing tool of laser engraver 3
Figure 2b: User input screen for engraving process parameters 3
Figure 3a: Scatter plot of power vs. speed for various specimens at 5 MPa 20
Figure 3b: Scatter plot of power vs. speed for various specimens at 3 MPa 21
Figure 3c: Scatter plot of power vs. speed for various specimens at 1 MPa 21
Figure 4a: Calculated best fit gradient for foaming experiments at 5 MPa 22
Figure 4b: Calculated best fit gradient for foaming experiments at 3 MPa 23
Figure 4c: Calculated best fit gradient for foaming experiments at 1 MPa 23
Figure 5a: SEM image of specimen foamed at 5 MPa, with 23% speed and 7% power 24
Figure 5b: A closer look at the microstructure at 5 MPa, with 23% speed and 7% power 25
Figure 5c: Surface micrograph of specimen foamed at 5 MPa, with 23% speed, 7% power 26
Figure 6: SEM image of specimen foamed at 5 MPa, with 30% speed and 7% power 27
Figure 7: SEM image of specimen foamed at 3 MPa, with 55% speed and 13% power 28
Figure 8: SEM image of specimen foamed at 1 MPa, with 46% speed and 10% power 29
Figure 9a: Original SEM image 30
Figure 9b: SEM image after adjusting the threshold 30
Figure 9c: Outline of cell areas traced, and cell numbers counted (in red) 31
Figure 10a: SEM image of specimen foamed at 5 MPa, with 15% speed and 5% power 32
Figure 10b: SEM image of specimen foamed at 5 MPa, with 17% speed and 5% power 32
Figure 10c: SEM image of specimen foamed at 5 MPa, with 19% speed and 5% power 33
Figure 11a: SEM image of specimen foamed at 3 MPa, with 50% speed and 10% power 34
Figure 11b: SEM image of specimen foamed at 3 MPa, with 50% speed and 13% power 34
Figure 12: Effective 'dot volume' considered 38
Figure 13a: Geometric pattern of foamed concentric circles 41
Figure 13b: Custom text can be written using this technique 41
Figure 13c: University of Washington insignia 41
Figure 14a: First foamed patch on PEI at 5 MPa, with 23% speed and 7% power 42
Figure 14b: Burnt foam on PEI at 5 MPa, with 23% speed and 9% power 42
Figure 14c: Burnt foam on PEI at 5 MPa, with 23% speed and 8% power 42
Figure 14d: Successful foam on PEI at 5 MPa, with 20% speed and 5% power 42
Figure 15: Additional foamed patches on PEI specimen saturated at 5 MPa 43
Figure 16: Different DPI settings foamed on one specimen 43
Figure A.17a: Full thickness micrograph of 5 MPa specimen, at 23% speed and 7% power 46
Figure A.17b: Oblique view near the top surface of specimen at 5 MPa, 23% speed and 7% power 47
Figure A.17c: Subsurface cross section of the specimen at 5 MPa, 23% speed and 7% power 47
Figure A.18a: Foamed cross section of 5 MPa specimen, at 15% speed and 5% power 48
Figure A.18b: SEM image of surface of 5 MPa specimen, at 15% speed and 5% power 48
Figure A.19a: Cross section of 5 MPa specimen, with 17% speed and 5% power 49
Figure A.19b: Uniform cell distribution of 5 MPa specimen, at 17% speed and 5% power 49
Figure A.20: Foamed cross section of 5 MPa specimen, with 19% speed and 5% power 50
Figure A.21a: Full thickness micrograph of 5 MPa specimen, with 30% speed and 7% power 50
Figure A.21b: SEM image of specimen cross section at 5 MPa, 30% speed and 7% power 51

Figure A.21c: Microcellular bubble distribution at 5 MPa, 30% speed and 7% power 51
Figure A.22a: SEM image of specimen cross section at 5 MPa, 35% speed and 8% power 52
Figure A.22b: SEM image of transition region at 5 MPa, 35% speed and 8% power 52
Figure A.23: Different microcellular locations of specimen at 3 MPa, 13% speed and 5% power..... 53
Figure A.24a: Full thickness micrograph for specimen at 3 MPa, 20% speed and 7% power 54
Figure A.24b: SEM micrograph of the foamed cross section at 3 MPa, 20% speed and 7% power..... 54
Figure A.24c: SEM image of transition region at 3 MPa, 20% speed and 7% power..... 55
Figure A.24d: Microcellular bubble distribution at 3 MPa, 20% speed and 7% power 55
Figure A.25a: Full thickness micrograph for specimen at 3 MPa, 40% speed and 10% power 56
Figure A.25b: SEM micrograph of the foamed cross section at 3 MPa, 40% speed and 10% power..... 56
Figure A.25c: Microcellular bubble distribution at 3 MPa, 40% speed and 10% power 57
Figure A.26a: Full thickness micrograph for specimen at 3 MPa, 55% speed and 13% power 58
Figure A.26b: Microcellular bubble distribution at 3 MPa, 55% speed and 13% power..... 58
Figure A.26c: SEM image of transition region at 3 MPa, 55% speed and 13% power..... 59
Figure A.27a: Full thickness micrograph for specimen at 1 MPa, 20% speed and 7% power 60
Figure A.27b: SEM image of specimen cross section at 1 MPa, 20% speed and 7% power..... 61
Figure A.27c: Microcellular bubble distribution at 1 MPa, 20% speed and 7% power 61
Figure A.28a: Full thickness micrograph for specimen at 1 MPa, 40% speed and 10% power 62
Figure A.28b: Microcellular bubble distribution at 1 MPa, 40% speed and 10% power..... 62
Figure A.29a: SEM image of specimen cross section at 1 MPa, 55% speed and 13% power 63
Figure A.29b: Microcellular bubble distribution at 1 MPa, 55% speed and 13% power..... 63
Figure A.29c: SEM image of transition region at 1 MPa, 55% speed and 13% power..... 64
Figure A.30a: Full thickness micrograph for specimen at 1 MPa, 46% speed and 10% power 64
Figure A.30b: Microcellular bubble distribution at 1 MPa, 46% speed and 10% power..... 65

List of Tables

Table 1: Exploratory foaming experiments at 5 MPa 4
Table 2: Exploratory foaming experiments at 3 MPa 12
Table 3: Exploratory foaming experiments at 1 MPa 16
Table 4: 5 MPa specimen parameters 27
Table 5: 3 MPa specimen parameters 28
Table 6: 1 MPa specimen parameters 29
Table 7: Effect of Speed on average cell size 33
Table 8: Effect of power on average cell size at 3 MPa 35

Acknowledgements

I would like to thank and express my sincere gratitude to Professor Vipin Kumar for encouraging me to pursue research at the Masters level, and for guiding and supporting me throughout this enriching journey. I would like to thank Professor Mohammad H. Malakooti for his innovative ideas, his help, and insightful suggestions throughout this endeavor. I would also like to thank Dr. John Weller for agreeing to be on my committee and offering his suggestions, expert knowledge and sharp observations pertaining to lasers and their effect on the resulting microstructure.

Throughout this research undertaking, I also had the chance to closely interact with other students whose efforts have made this work possible. I would like to thank Santhosh Sridhar for his help with the pressure vessel operation, as well as his fresh perspective on possible avenues of thought when planning experiments at various points during my thesis. I would also like to thank Conrad Ciszek for his support during my thesis, and Guanning He, especially with their continuous assistance in the operation of the laser engraver. I would also like to thank Scott Braswell, a research scientist at the Molecular Analysis Facility, for helping me acquire a variety of micrographs that are included within and analyzed in this body of work.

I would also like to acknowledge my parents, who have encouraged me at every stage of my life. Their relentless support of my ambition, and belief in me has motivated me through difficult times and helped to keep me focused on the task at hand.

Chapter 1.0 Introduction

The concept of introducing bubbles into plastics and creating microcellular plastics was developed during the 1980's [1-2], with polystyrene and nitrogen gas to induce bubble nucleation. Prof. Nam. P. Suh was one of the pioneers to study the concept from a process design and manufacturing perspective. Since then, the concept was tested on and expanded to different polymers, mainly thermoplastics aiming at different practical applications.

Professor Vipin Kumar and John Weller (Ph.D. 1996) applied the concept on Polycarbonate (PC) and studied the effects of different process parameters. There are two basic steps in the process to make microcellular foams. In the first step the polymer specimen is placed in a pressure vessel and subjected to a high pressure gas. After saturation with gas the specimen is removed from the pressure vessel. In the second step, the specimen is heated to a temperature near the glass transition temperature of the polymer, where a large number of bubbles nucleate, creating a microcellular structure. The principle is that the instability caused due to the sudden reduction in gas solubility as the saturated polymer is heated (increase in temperature), acts as the driving force to nucleate bubbles. Since the polymer is essentially in a solid state during processing, this process has become known as the "solid-state process" to make microcellular foams. The solid-state process has been used to create microcellular foams in several amorphous and semi-crystalline thermoplastics such as PVC [3], PC [4], ABS [5], PET, PETG, and CPET [6-8], to name a few. The interest in microcellular foams has been largely driven by the potential to reduce the amount of plastic needed by reducing the polymer density, especially for thin-walled packaging applications. In the past decade or so, the cell size has seen a reduction by over two orders of magnitude, to order 100 nm, and nanofoams have been created in various types of polymers using the solid-state process where the gas saturation step is carried out below room temperature [9-11].

The idea to introduce the bubbles selectively, rather than in the bulk, has been touched upon occasionally, and never really explored in depth. Handa et al [12] described a stress-induced nucleation process and demonstrated the possibility for selective nucleation of bubbles, in areas where a high stress is applied to a gas-saturated polymer specimen. In this study we explore cell nucleation using a laser beam and present the preliminary result on polycarbonate. The laser beam gives exceptional control on where the cells nucleate, and we hope that this capability will lead to many unique and novel applications in future.

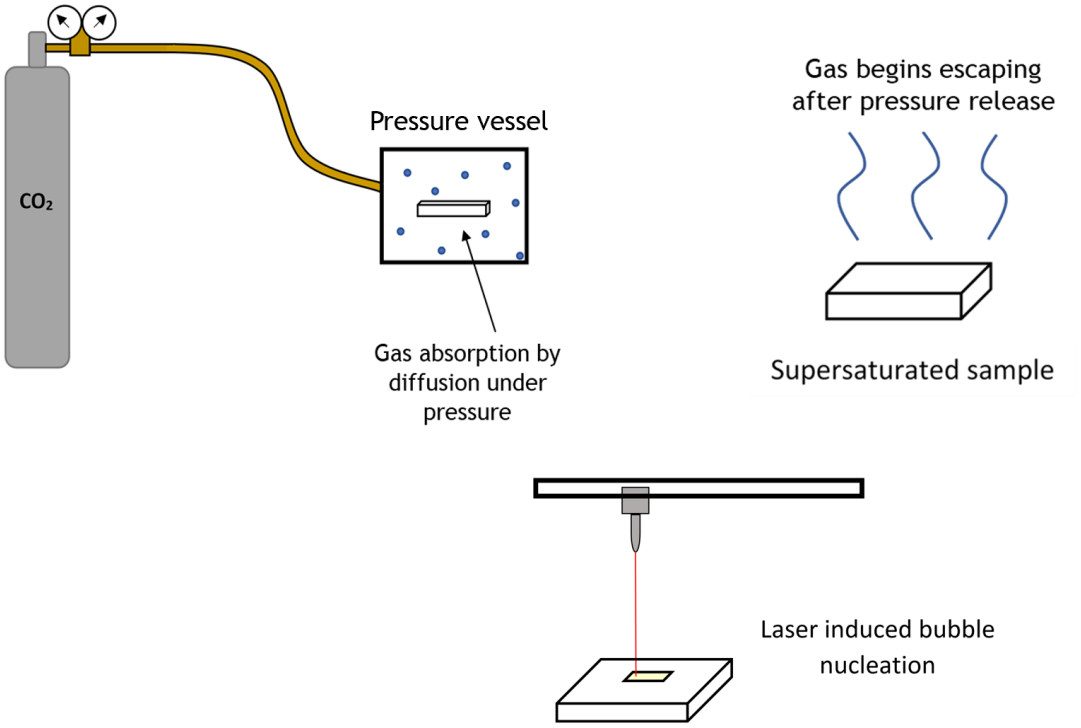

Figure 1: Process Schematics

1.1 Goals and Motivation:

The overarching goal of this project was to demonstrate the feasibility of a novel approach to induce microcellular foaming in polycarbonate specimens. The key aspect of this approach is the extraordinary flexibility offered to the user to determine the locations on the specimen to be foamed, as well as any complex geometries to be foamed. This is not possible with the current processes being used, like the hot oil bath and hot press, which foams the entire specimen and gives no control to the researcher.

The initial goal was to find a relationship between the speed and power settings of the laser engraver system to cause foaming in polycarbonate samples saturated with carbon dioxide. A "successful" foam would be identified as a white patch on the polycarbonate specimen.

The next step, after achieving foaming using the laser engraver, would be to study the microstructure of these samples with the help of SEM (scanning electron microscope) imaging and study the corresponding morphology, like bubble size and distribution within each sample, and how this is affected by some of the variables in this experiment, like the saturation pressure, speed and power settings of the laser engraver.

Chapter 2.0 Process Space Exploration

2.1 Procedure and Experiments Performed

Polycarbonate samples were cut using a shear and their dimensions measured using digital calipers. Next, they were saturated with carbon dioxide gas at 5 MPa using a pressure vessel. The time taken to saturate the samples, based on a nominal thickness of 1.5 mm, was calculated to be approximately 65 hours, based on the sorption plot from John Weller's thesis [13]. After removal from the pressure vessel, specimens were weighed using a precision mass balance prior to foaming, to obtain the CO_2 gas concentration.

For the laser engraving process, the focal point was manually set using a focus tool attachment (~41.46 mm height) to the surface of each individual PC sample (**Figure 2a**). Corel Draw 2020 was used to enter the speed and power parameters under 'Raster', with a center engraving setting chosen for all specimens exposed to the laser beam (**Figure 2b**). Raster is used for jobs involving engraving, whereas the Vector setting is used to cut shapes out of materials and is therefore not applicable for this study.

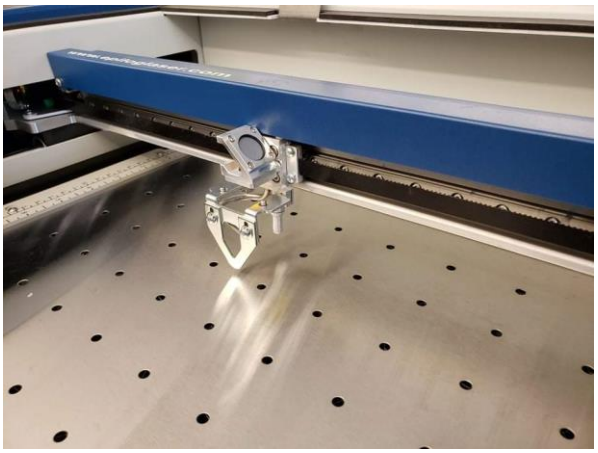

Figure 2a: Focusing tool of laser engraver. The focus is set by establishing contact with the end of the fixture and the specimen surface to be engraved.

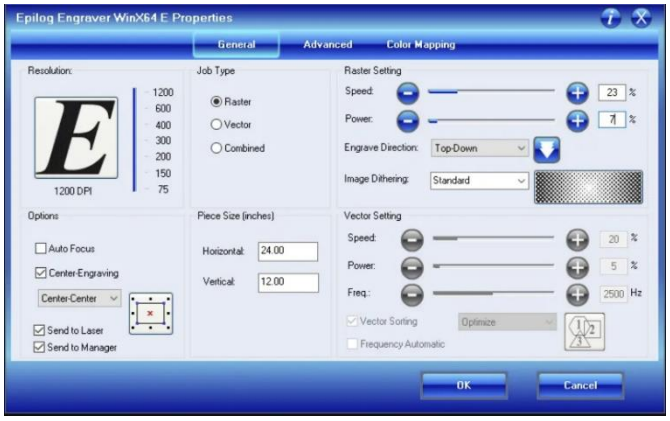

Figure 2b: User input screen for engraving (foaming) process parameters.

Initial experiments were carried out to find the speed and power settings of the laser engraver to generate a white, opaque foamed patch on the polycarbonate samples. All the speed and power settings are expressed as percentage values of the maximum setting. The maximum speed (100%) is **82 inches/second** and maximum power (100%) is **40 W**. The DPI (dots per inch) setting throughout this study for all samples considered was kept fixed at its maximum value of **1200**.

The following section provides tabulated records of the experiments performed at various saturation pressures. The results are discussed and categorized into the process window observations from the graph plots, discussed in Section 2.3, and the microstructure observations for selected specimens, discussed in Chapter 3.

2.2 Experimental catalog of foaming experiments at 1, 3 and 5 MPa:

At saturation pressures of 5, 3 and 1 MPa, several exploratory experiments were conducted to determine if the process of 'engraving' a foam using a laser beam was feasible or possible, and to ascertain if any trend or process window could be obtained for this novel technique. The preliminary results are discussed after this section.

Table 1: Exploratory foaming experiments at 5 MPa

Specimen ID	CO_2 gas conc. (g/g %)	Speed (%)	Power (%)	t_{foam} (s)	Foamed patch dimensions - length x width (cm x cm)	Figure
1	-	2	5	680	7 x 0.5	 Front view  Rear view
2	-	5	3	139	5 x 0.3	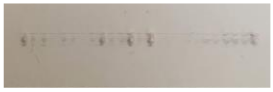 Front view - Faint line observed at 3% power
3	10.77*	15	5	54	2 x 0.5	 Front view  Rear view

4	10.67*	17	5	50	2 x 0.5	 Front view  Rear view
5	10.62*	19	5	46	2 x 0.5	 Front view  Rear view
6	10.16*	17	7	50	2 x 0.5	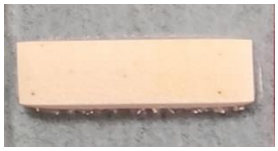 Front view  Rear view
7	10.30*	23	7	40	2 x 0.5	 Front view

						 Rear view
8	10.36*	30	10	35	2 x 0.5	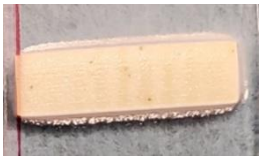 Front view 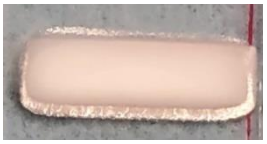 Rear view
9	10.15*	20	8	45	2 x 0.5	 Front view  Rear view
10	10.11*	20	7	45	2 x 0.5	 Front view  Rear view

11	10.43*	35	10	25	1.5 x 0.5	 Front view  Rear view
12	10.35*	40	10	23	1.5 x 0.5	 Front view  Rear view
13	10.22*	45	13	23	1.5 x 0.5	 Front view  Rear view

14	10.09*	55	13	23	1.5 x 0.5	 Front view 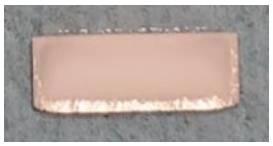 Rear view
15	10.03*	70	15	23	1.5 x 0.5	 Front view  Rear view
16	10.84*	20	20	20	2 x 0.3	 Front view  Rear view

17	9.36^{+}	25	5	31	1.5 x 0.5	 Front view  Rear view
18	9.24^{+}	30	7	28	1.5 x 0.5	 Front view  Rear view
19	9.14^{+}	30	8	29	1.5 x 0.5	 Front view  Rear view
20	8.96^{+}	35	8	26	1.5 x 0.5	 Front view  Rear view

21	8.83^{+}	45	10	23	1.5 x 0.5	 Front view  Rear view
22	9.08^{+}	10	4	64	1.5 x 0.5	 Front view  Rear view
23	8.87^{+}	8	5	78	1.5 x 0.5	 Front view  Rear view
24	8.80^{+}	10	6	64	1.5 x 0.5	 Front view

						 Rear view
25	8.65+	15	6	45	1.5 x 0.5	 Front view  Rear view
26	8.51+	22	6	34	1.5 x 0.5	 Front view  Rear view

* *Gas concentration immediately after saturation (Equilibrium gas concentration)*

+ Gas concentration just prior to foaming

Table 2: Exploratory foaming experiments at 3 MPa

Specimen ID	CO_2 gas conc. (g/g %)$^+$	Speed (%)	Power (%)	t_{foam} (s)	Foamed patch dimensions - length x width (cm x cm)	Figure
1	6.36	13	5	51	1.5 x 0.5	 Front view  Rear view
2	6.22	19	5	37	1.5 x 0.5	 Front view  Rear view
3	6.14	20	7	36	1.5 x 0.5	 Front view  Rear view

4	6.06	40	10	25	1.5 x 0.5	 Front view  Rear view
5	6.01	55	13	23	1.5 x 0.5	 Front view  Rear view
6	6.39	30	7	27	1.5 x 0.5	 Front view  Rear view
7	6.33	45	9	24	1.5 x 0.5	 Front view

						 Rear view
8	6.19	30	10	28	1.5 x 0.5	 Front view  Rear view
9	6.09	50	10	23	1.5 x 0.5	 Front view  Rear view
10	5.96	50	13	25	1.5 x 0.5	 Front view  Rear view

11	6.45	25	6	32	1.5 x 0.5	 Front view  Rear view
12	6.40	35	8	26	1.5 x 0.5	 Front view  Rear view
13	6.29	20	9	36	1.5 x 0.5	 Front view  Rear view
14	6.22	30	11	28	1.5 x 0.5	 Front view

						 Rear view

+ Gas concentration just prior to foaming

Table 3: Exploratory foaming experiments at 1 MPa

Specimen ID	CO_2 gas conc. (g/g %)+	Speed (%)	Power (%)	t_{foam} (s)	Foamed patch dimensions - length x width (cm x cm)	Figure
1	2.91	13	5	51	1.5 x 0.5	 Front view  Rear view
2	2.86	19	5	38	1.5 x 0.5	 Unfoamed specimen under applied settings
3	2.83	20	7	36	1.5 x 0.5	 Front view

						 Rear view
4	2.82	40	10	24	1.5 x 0.5	 Front view  Rear view
5	2.79	55	13	24	1.5 x 0.5	 Front view  Rear view
6	2.61	24	6	33	1.5 x 0.5	 Front view  Rear view

7	2.57	31	8	27	1.5 x 0.5	 Front view  Rear view
8	2.51	46	10	24	1.5 x 0.5	 Front view  Rear view
9	2.50	17	9	41	1.5 x 0.5	 Front view  Rear view

10	2.55	27	11	29	1.5 x 0.5	 Front view  Rear view

+ Gas concentration just prior to foaming

2.3 Discussion of experimental results at different pressures:

A wide spectrum of foams was obtained from varying the speed and power. A bright white foam was obtained, indicating a perfectly foamed specimen, and was the visual indicator of success in these exploratory experiments (for e.g. specimen IDs 5 and 18 in Table 1). Other types of foams obtained were either characterized by a melted or burnt appearance, i.e. yellow/caramel or occasionally black patches on the specimen area engraved, (in an extreme case the surface had been gouged/peeled open by the laser, like specimen ID 16 in Table 1) or a striped pattern showing signs of transparency or incomplete foaming (for e.g. specimen ID 2 in Table 2 and specimen ID 6 in Table 3). An interesting observation for some of the burnt specimens was the 'fade out' near the top edge of the engraved patch (for e.g. specimen ID 9 in Table 3), which was likely the burnt deposits of PC particles on the surrounding area of the specimen.

The specimens were also turned over and the rear side of the foam was observed. It was interesting to note that the first specimen in Table 1 had been locally burnt on the surface exposed to the laser, but it had foamed underneath, according to the second image in row 1 of Table 1. It became a factor of interest to check for all the specimens if experienced the same effects throughout their foamed depth, or whether there was any physical change in foams produced from the side of the surface exposed to the laser beam to the sub-surface protected from direct heating by the laser.

Altering the saturation pressure did not have an immediately discernible effect on the type of foams produced, but the range of settings inducing successful foams seemed slightly altered each time. It was intuitively determined that there could possibly be a pattern of these settings that causes these white foams to be generated. Therefore, to confirm this hypothesis, these results were plotted on graphs, to better highlight any trends observed and draw some further insights (**Section 2.4**).

2.4 Process Window Plots at 1, 3 and 5 MPa CO_2 saturation pressures

To summarize from the previous section, polycarbonate specimens were saturated with CO_2 at 1, 3 and 5 MPa pressures, and subsequently foamed in the laser engraver at arbitrary speed and power settings. A range of settings were tested on specimens, and the results were categorized by a simple visual indication of the appearance of the specimen, i.e. whether it had successfully 'foamed', burnt/completely melted, or partially foamed. The important result that was focused on was only the combination of settings that yielded successful foams.

A graph of Power vs. Speed was plotted on Python, incorporating the distribution of speed and power data points tested over the course of this project (**Figure 3a**). A clear process window was observed between the speed and power settings at 5 MPa for the foamed specimens. Increasing the power too much (above the process window region) caused the samples to melt and get burned, whereas increasing the speed too much (under the process window region) resulted in an incomplete foaming pattern.

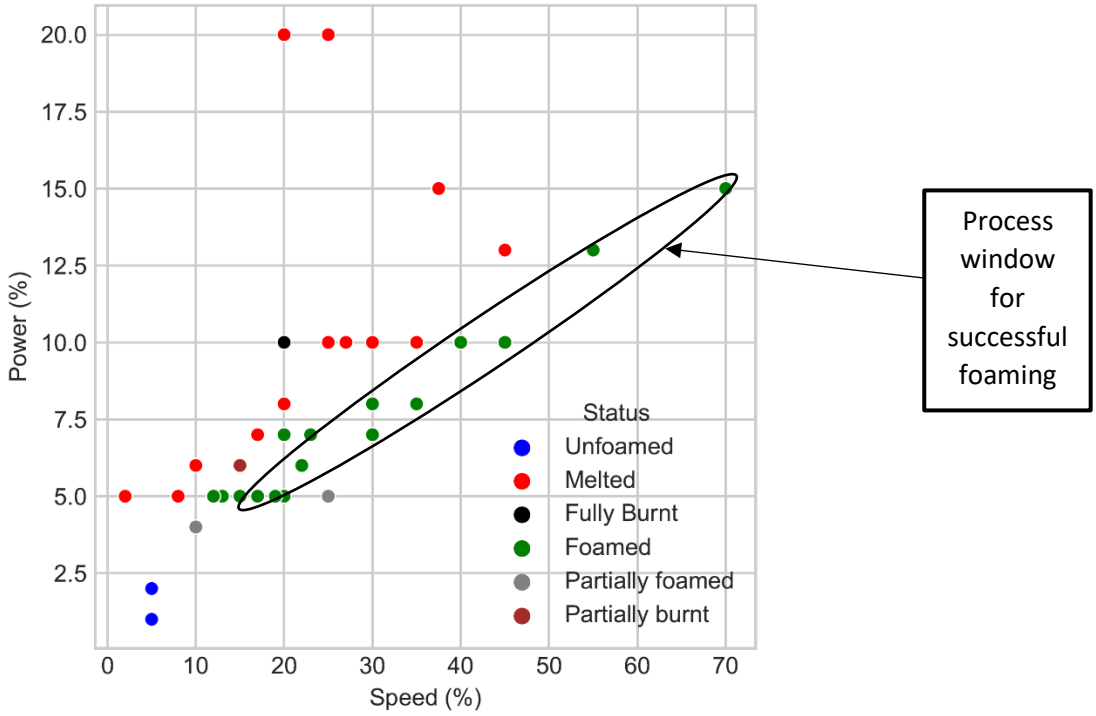

Figure 3a: Scatter plot of power vs. speed for various specimens at 5 MPa

Similar results at lower saturation pressures were graphed on Python (**Figures 3b and 3c**).

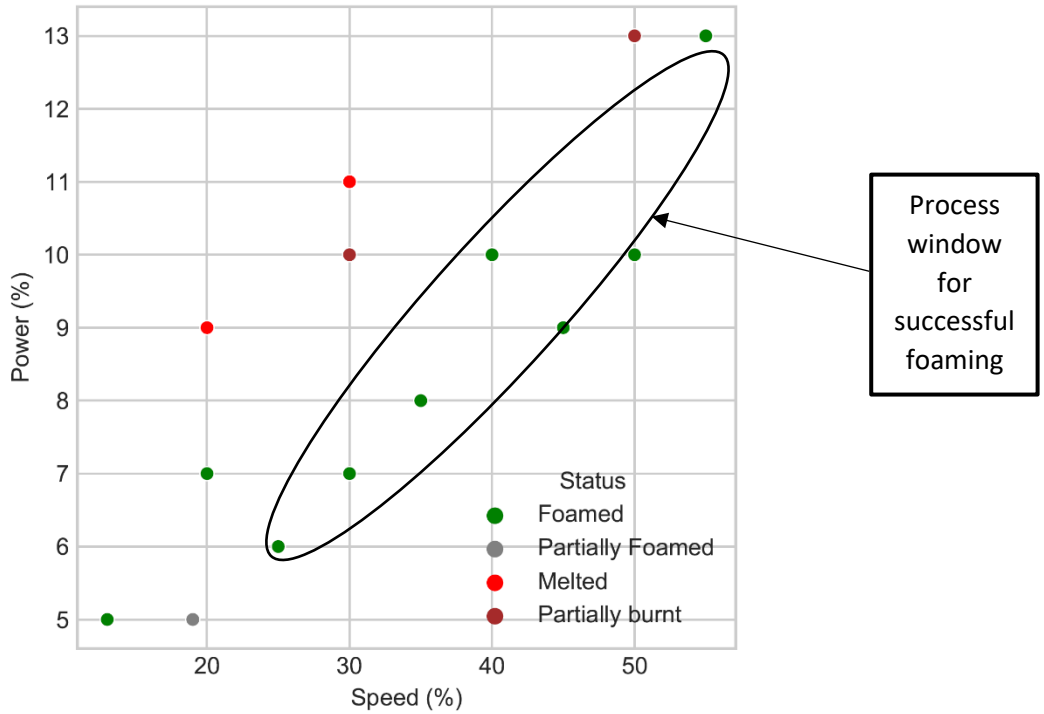

Figure 3b: Scatter plot of power vs. speed for various specimens at 3 MPa

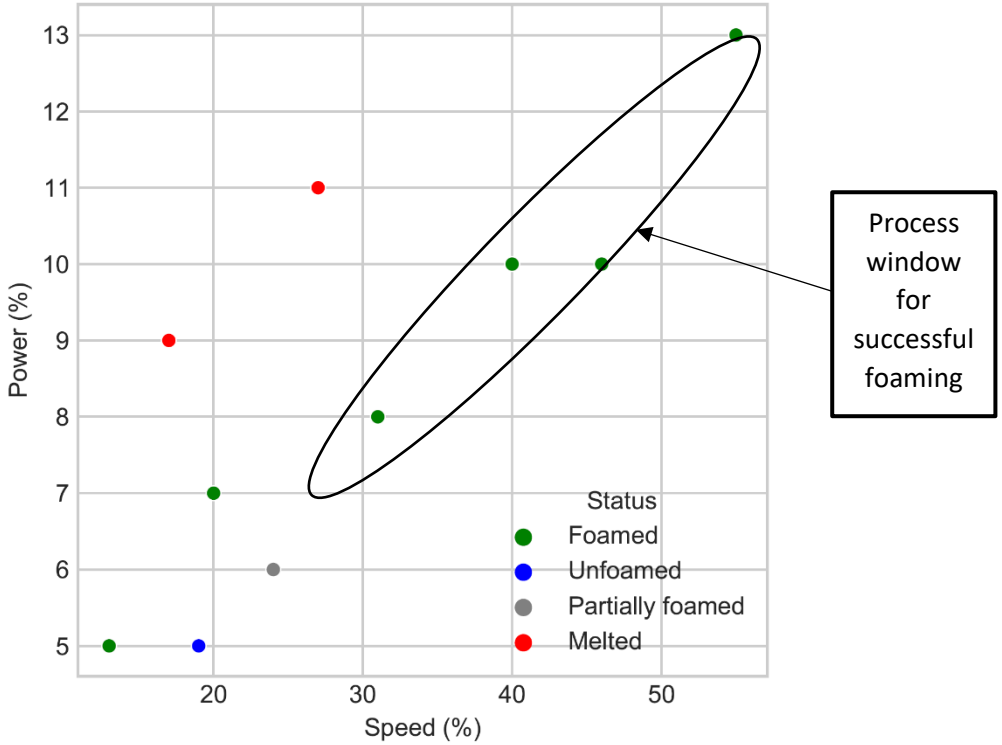

Figure 3c: Scatter plot of power vs. speed for various specimens at 1 MPa

An expected outcome validated by the graph plots was the 'reducing' process window or narrower range of speed and power settings that could be applied to create foams (green dots), as the saturation pressure dropped. The process window is clearly shifting to the top right hand side, comparing the graphs in **Figures 3b and 3c** (their axes have the same scale).

However, we could still observe a clear relationship between the general trends of power and speed of specimens that had successfully foamed. After isolating the 'foamed' (green) coordinates from each of the graphs, linear regression was used to plot a best fit line and calculate its gradient. This gives us:

Gradient $m = \frac{Power}{Speed} = Linear\ energy\ density$ or energy transferred per unit length

With units of: $\frac{J/s}{m/s} = \frac{J}{m}$

For the 5 MPa plot, m = 3.52 J/m

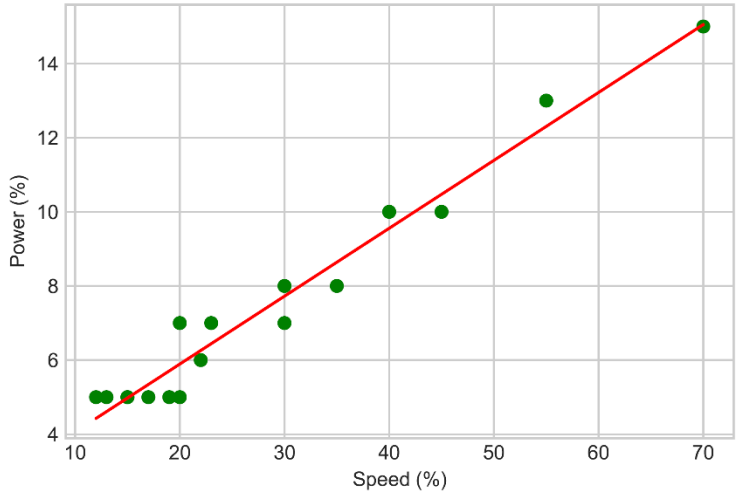

Figure 4a: The calculated best fit gradient for 17 data points was 3.52 J/m

For the 3 MPa plot, m = 3.00 J/m

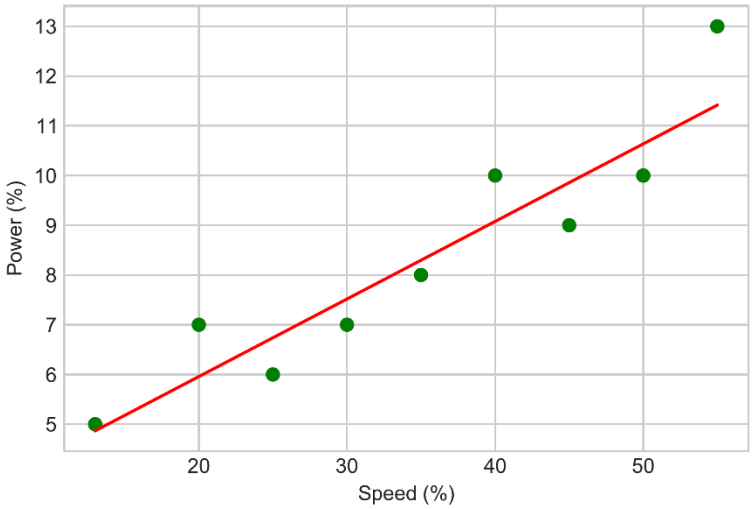

Figure 4b: The calculated best fit gradient for 9 data points was 3.00 J/m

For the 1 MPa plot, m = 3.29 J/m

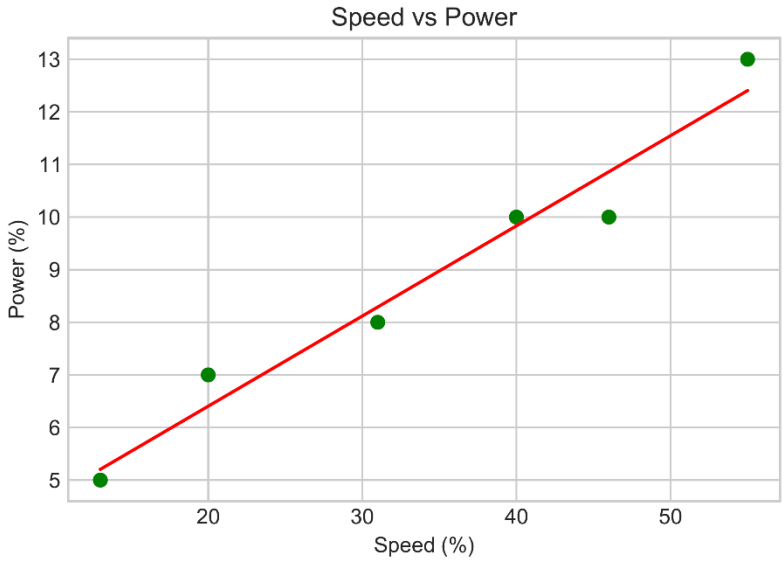

Figure 4c: The calculated best fit gradient for 6 data points was 3.29 J/m

From these results we can see a close conformance in gradient values, indicating that the energy per unit length required to induce foaming might be dependent on the saturation pressure of the specimens. However, this would have to be investigated further as the number of data points across the three pressures are not equal. Therefore, it would be recommended to conduct more experiments at 3 MPa and 1 MPa or use Design of Experiments to predict a more accurate trend to be measured across all three plots.

As expected, we can also see evidence of a reducing process window as the pressure decreases, which is something to be expected, since the available CO_2 gas concentration decreases from approximately 9% to 6% to 2.5%, referring to the tabular data for CO_2 gas concentration prior to foaming, at various saturation pressures (**Section 2.2**).

Chapter 3.0 Foam Microstructure

The foamed specimens at various pressures of 1, 3 and 5 MPa were fractured in liquid nitrogen and studied under a Scanning Electron Microscope (SEM). From **Figure 5a**, it was immediately apparent that the top surface of the foams showed signs of being melted by the laser, (before it resolidified), due to the rough undulations clearly visible. Solid state foaming is achieved under this melted and resolidified top layer as evidenced by the microstructural distribution of bubbles (**Figure 5b**).

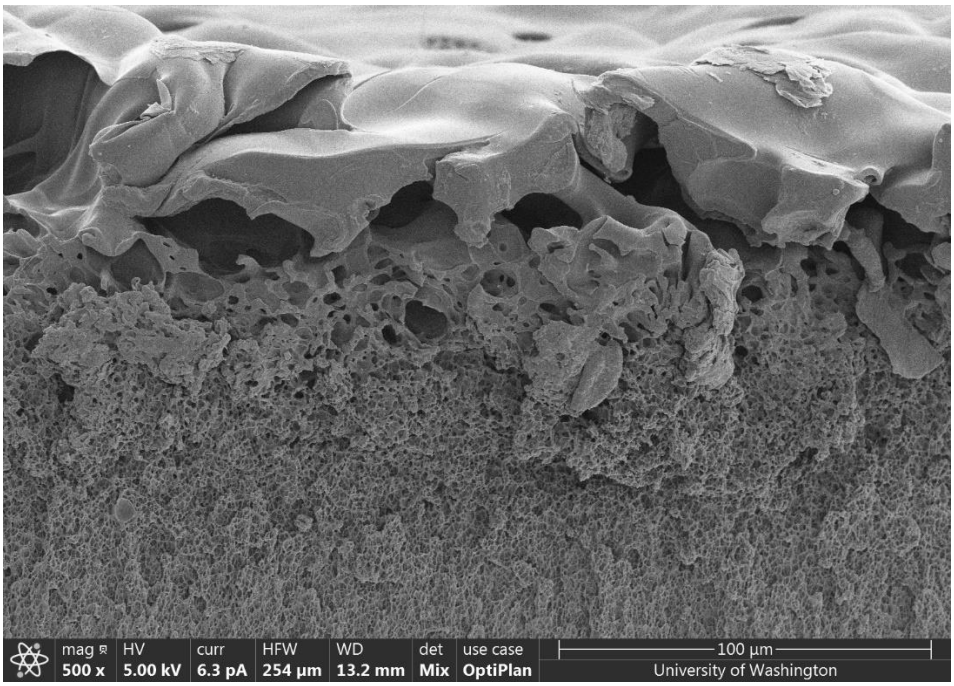

Figure 5a: This specimen was foamed at 5 MPa, with 23% speed, and 7% power. The surface has melted and re-solidified, indicating a sharp contrast with the oil bath and hot press techniques which generate an unfoamed skin on the top surface. This is an interesting change, peculiar to the laser induced foaming technique. Under this melted surface layer, we see the presence of microcellular foams (next Figure).

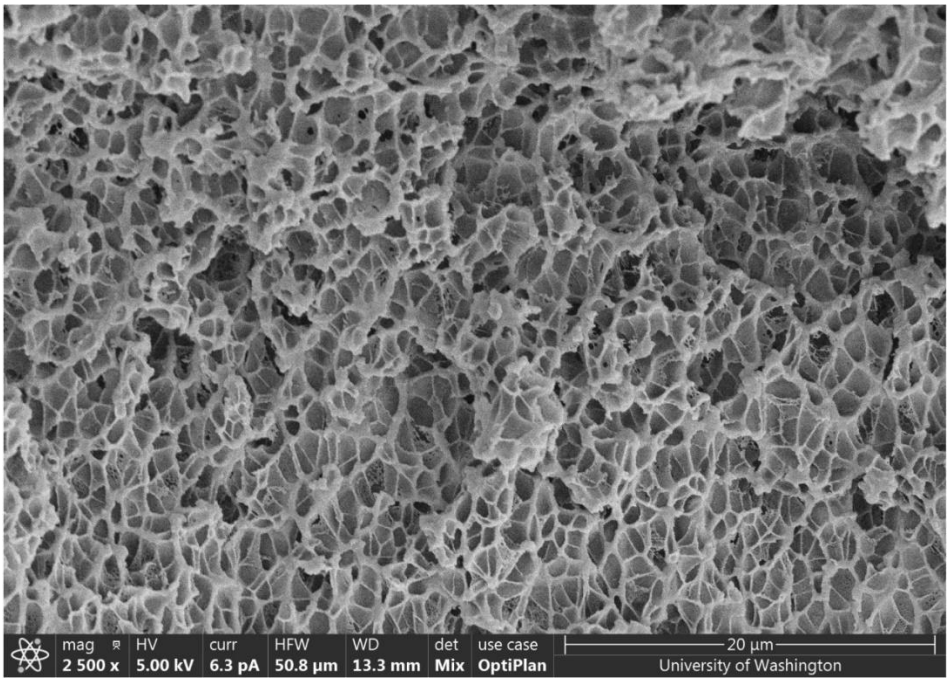

Figure 5b: A closer look at the microcellular foam. A fine distribution of microcellular bubbles is produced under the melted surface thickness, courtesy of solid state foaming. The bubbles produced are extremely small, and appear to range from 2-3 microns

Another feature of note was the porous morphology of the surface of the same specimen (**Figure 5c**). This surface which appeared to be a solid, unbroken patch at the macroscopic scale, had numerous holes when magnified 500x under the microscope. These holes are likely caused due to escaping CO_2 gas as the surface is being melted by the laser beam. This raises a question about whether the holes could be connected to the underlying cell microstructure. Perhaps this technique could be used to create open celled structures?

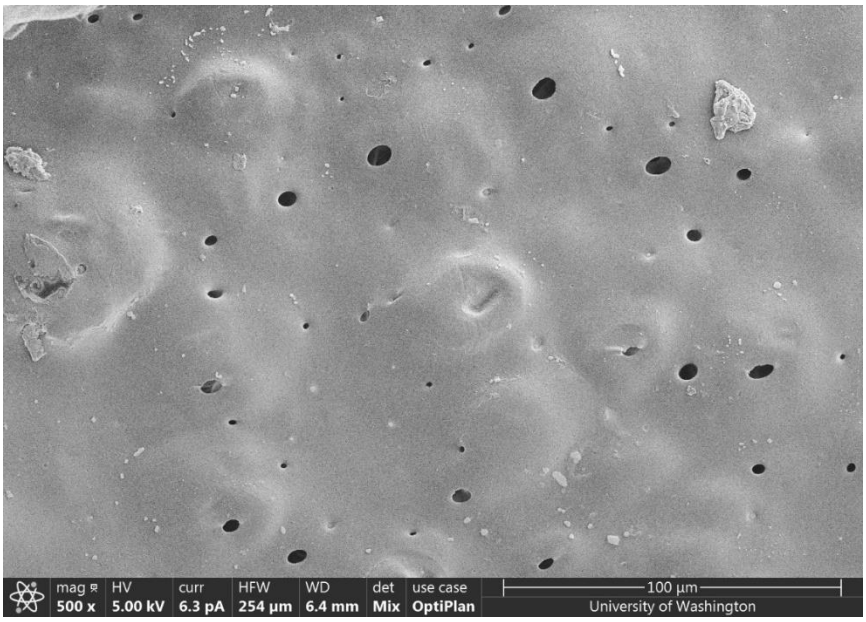

Figure 5c: The micrograph depicts a surprisingly porous morphology for the melted surface. These holes are likely caused due to the escaping CO_2 gas as the specimen is being heated by the laser.

Four parameters were analyzed in specimen micrographs at 1, 3 and 5 MPa:

1. Melted surface thickness
2. Depth of foamed region
3. Average cell size within the uniform cell distribution (see **Section 3.1**)
4. Cell size range (from under the melted surface layer till the 'transition' region, where the microstructure transitions to solid polycarbonate)

As mentioned before, from **Figure 5a**, we see that this novel laser processing technique melts the surface whereas the existing techniques like the oil bath and hot press, produce a solid, unfoamed skin. Hence, it is of interest to measure this melted surface thickness and study its relation (if any) to the processing parameters as it represents an effective 'skin' for laser induced foaming. The remaining parameters like foam depth, average cell size, and cell size range help quantify the primary region of focus, which is the microcellular foam generated. An average of 10 readings for the melted surface thickness and foam depth was taken along the cross section of the specimen.

5 MPa micrograph:

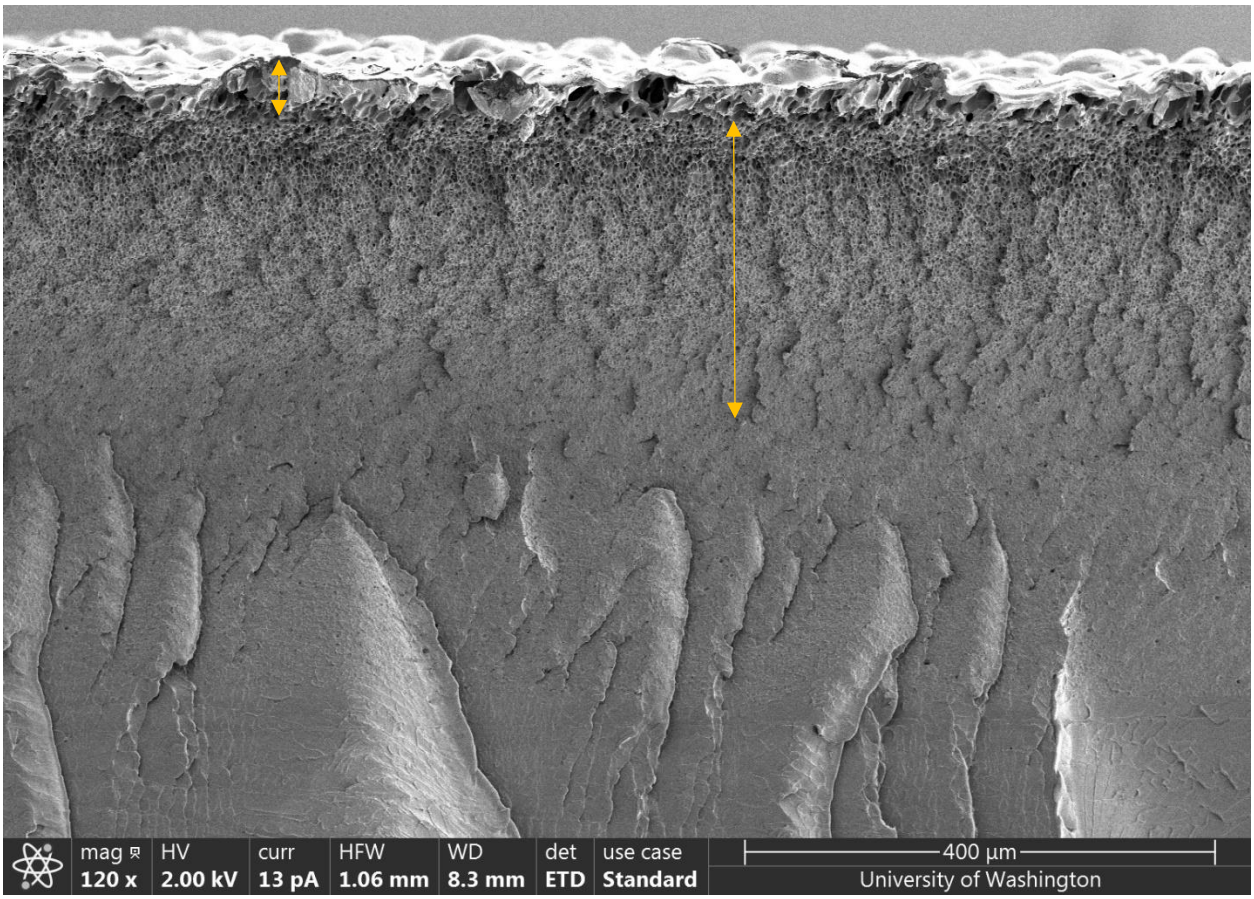

Figure 6: Specimen foamed at 30% speed and 7% power

Table 4: 5 MPa specimen parameters

Melted surface thickness	**30 microns**
Foam depth	**216 microns**
Average cell size	**1.83 microns**
Cell size range	**5.55 microns to 1.20 microns**

3 MPa micrograph:

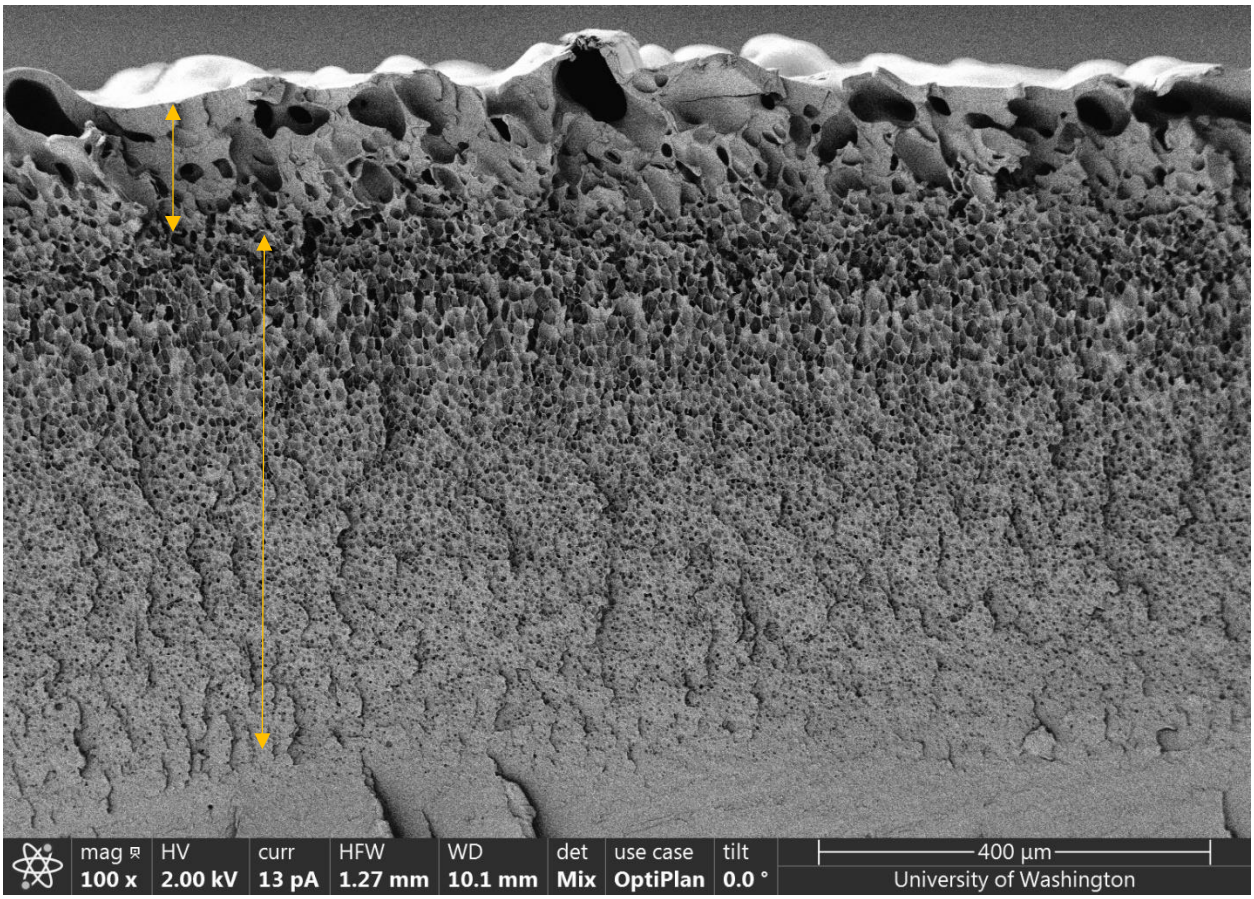

Figure 7: Specimen foamed at 55% speed and 13% power

Table 5: 3 MPa specimen parameters

Melted surface thickness	**120 microns**
Foam depth	**550 microns**
Average cell size	**1.90 microns**
Cell size range	**9.01 microns to 1.25 microns**

1 MPa micrograph:

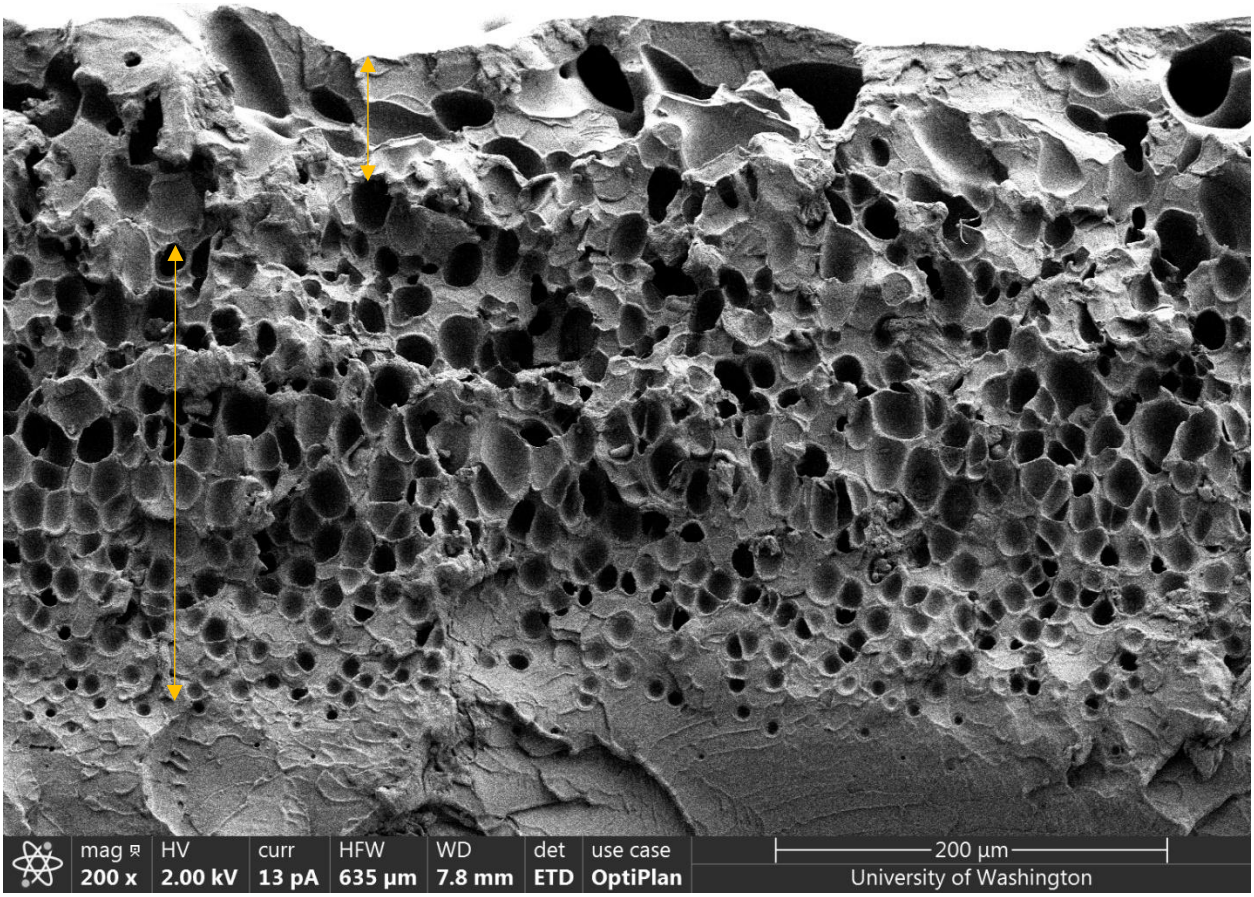

Figure 8: Specimen foamed at 46% speed and 10% power

Table 6: 1 MPa specimen parameters

Melted surface thickness	**73 microns**
Foam depth	**230 microns**
Average cell size	**8.27 microns**
Cell size range	**19.83 microns to 6.84 microns**

3.0.1 Observations from SEM micrographs

The melted surface thickness appears to be directly proportional to the power and does not seem to be influenced much by the speed, or the saturation pressure. The general trend indicates that the average bubble size increases as the saturation pressure decreases, which is expected. However, an interesting result was that the 3 MPa and 5 MPa foams yielded similar cell sizes. This implies that for 3 to 5 MPa pressures, careful selection of speed and power settings could possibly generate similar bubbles, irrespective of the pressure variation. This is surprising because the saturation pressure was expected to be the overarching factor that controls cell size, though this appears to be not the case.

A general conclusion we could make is from the results is that a wide range of average cell sizes can be obtained through manipulating the speed and power settings.

3.1 Average cell size measurement method using ImageJ

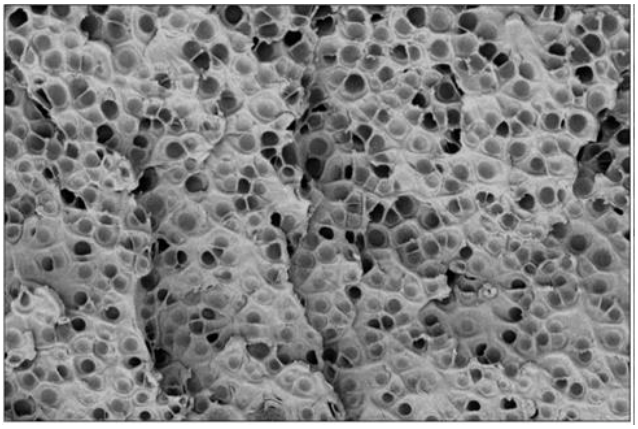

Figure 9a: Original SEM image

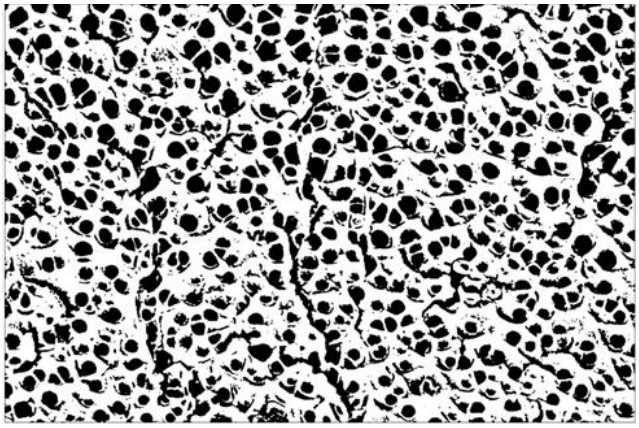

Figure 9b: After adjusting the threshold

First, the image is scaled, and then a filter is applied to it to set the range of cell sizes to be resolved by the software. To this filtered image, an arbitrary threshold is set by adjusting a bar (using trial and error) to shade the bubble regions whose areas need to be measured (black portions in **Figure 9b**). This generates an overlay (**Figure 9b**). The area distribution is then analyzed for this overlay (**Figure 9c**), and the values for individual cells are exported to an Excel file.

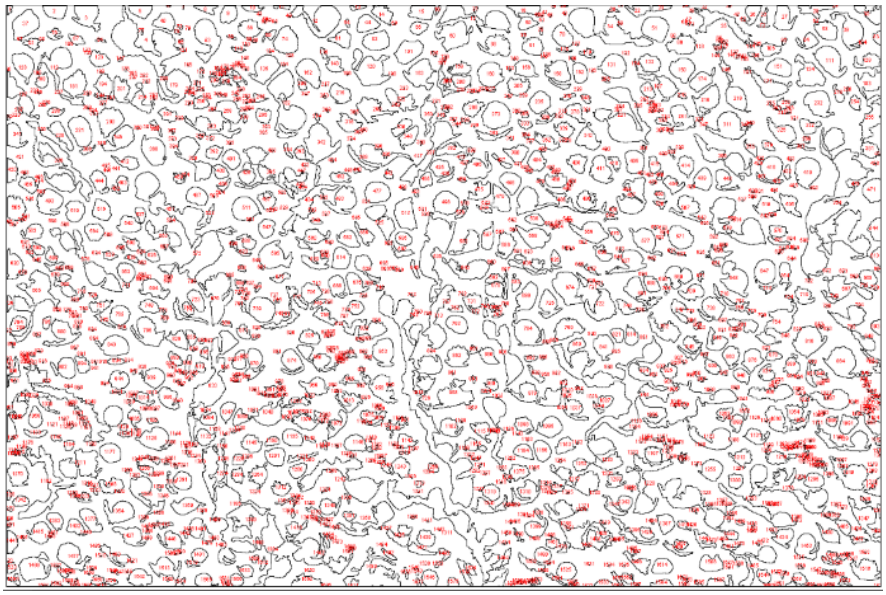

Figure 9c: Outline of cell areas traced, and cell numbers counted (in red)

3.1.1 Limitations of this process

This method sometimes combines separate cell areas to be measured, or conversely treats additional artefacts from the SEM as cell areas to be measured. Additional cleaning is recommended for images in order to obtain a more accurate representation of the areas measured. Cleaning includes manually erasing artefacts from the processed image so that factors which can cloud the readings are not considered.

To find the average cell size (diameter), the cell areas were assumed to be circular, although they have irregular shapes. The individual cell diameters were found using this approximation, before taking an average of all these diameter measurements to obtain a final average diameter.

However, despite these limitations and approximations, just by comparing the final calculated value for cell size with the scale bar attached to each SEM image, this served as a sanity check to ensure that the results obtained were fairly reasonable.

3.2 Variation of structure (average cell size) with speed at 5 MPa

At 5 MPa saturation pressure and a fixed power of 5%, different speeds of the laser were applied to 3 different polycarbonate specimens that had successfully foamed, and the effect on average cell size due to speed was investigated.

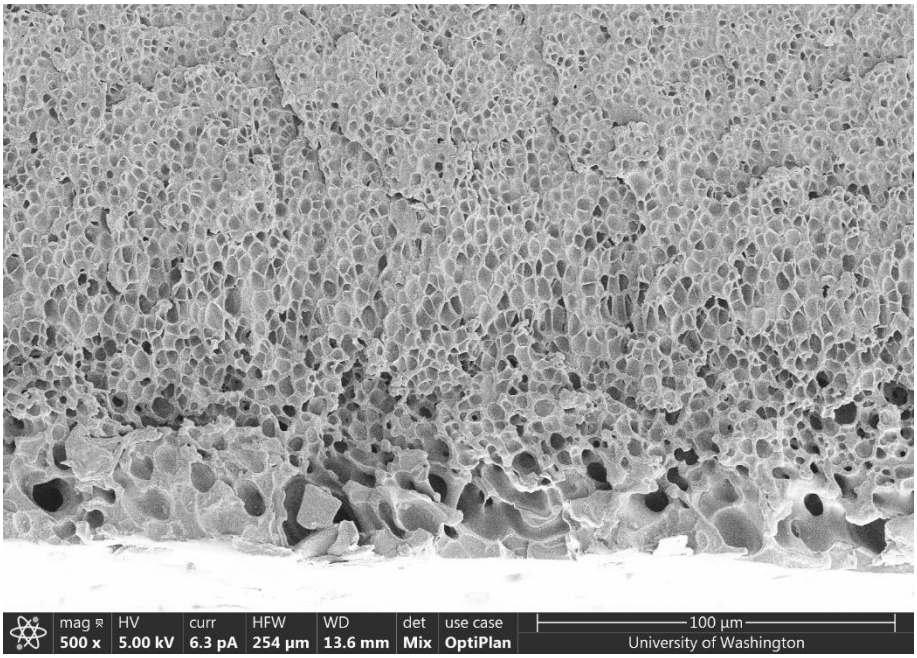

Figure 10a: 15% speed, 5% power

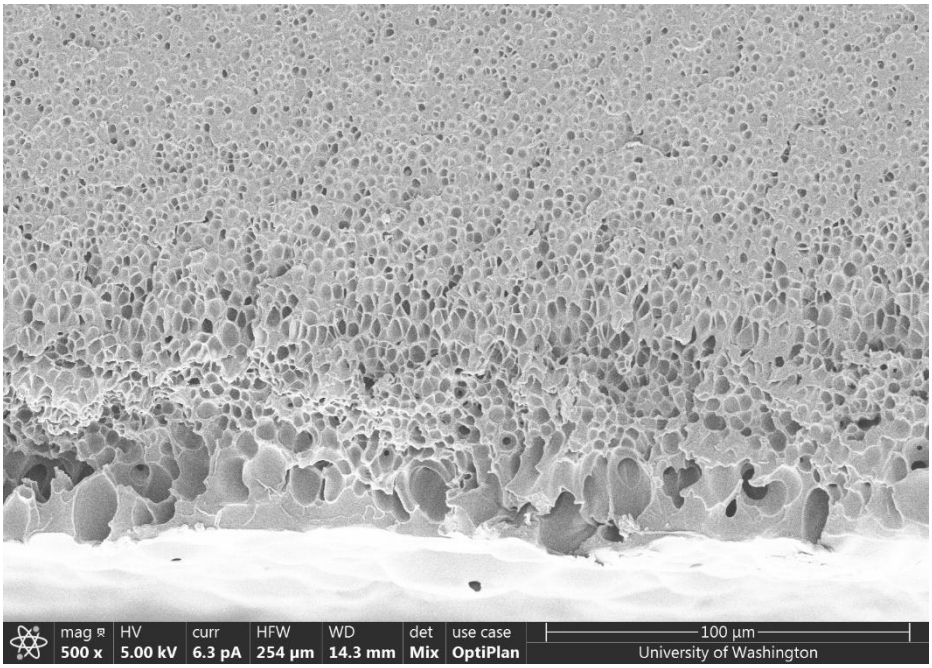

Figure 10b: 17% speed, 5% power

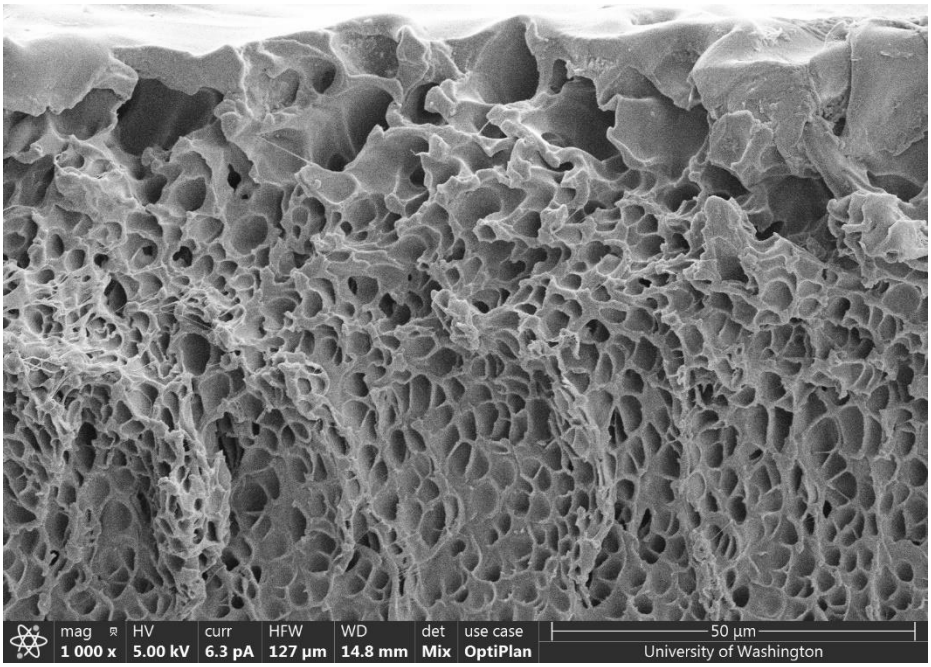

Figure 10c: 19% speed, 5% power

Table 7: Effect of Speed on average cell size

Specimen parameters		Average cell size (microns)
Speed (%)	Power (%)	
15	**5**	**1.69**
17	**5**	**1.53**
19	**5**	**1.31**

Observations:

From these results we can see a clear trend in the average cell size. The cell size decreases with an increase in speed (other factors remaining constant). This is an intuitive inference, since we would expect a higher speed to lead to lower overall (thermal) energy delivered to the specimen by the laser beam. Lower energy indicates that individual cells nucleate to a smaller extent, which is corroborated by the values provided in the Table above.

3.3 Variation of structure (average cell size) with power at 3 MPa

At a 3 MPa saturation pressure, two specimens were chosen to study the effect on average cell size of varying the power delivered by the beam, while keeping the speed constant. The results are discussed below.

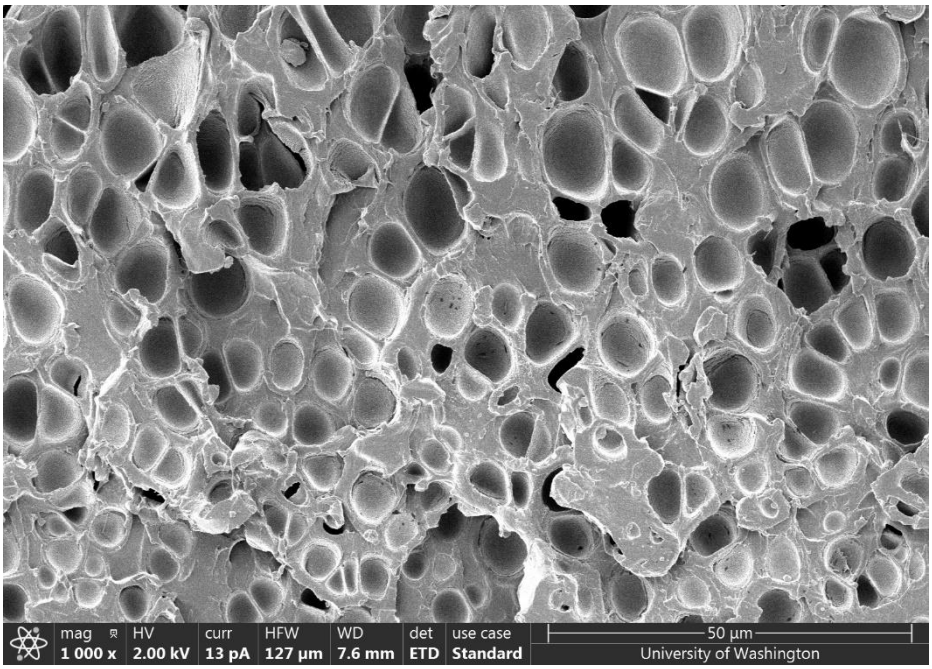

Figure 11a: 50% speed, 10% power

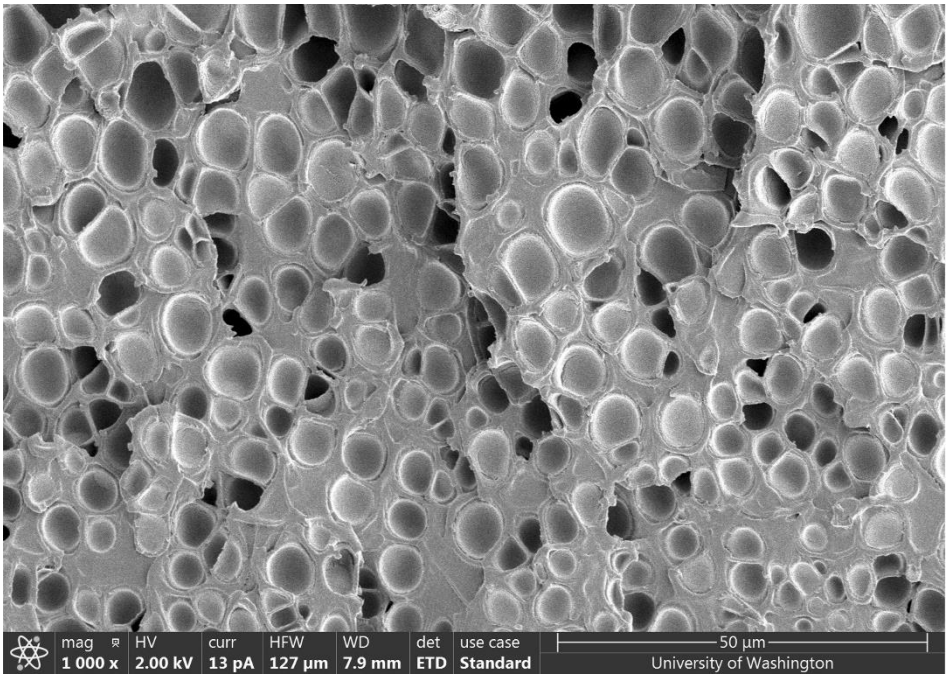

Figure 11b: 50% speed, 13% power

Table 8: Effect of power on average cell size at 3 MPa

Specimen parameters		Average cell size (microns)
Speed (%)	Power (%)	
50	**10**	**9.09**
50	**13**	**6.78**

Observations:

These results indicated a decreased cell size for an increased laser power, all other factors remaining constant. This seemed counterintuitive, since we would have expected the increased power, to increase the average bubble growth. However, a different perspective was borne from this result, which is that the melted surface layer (which is directly dependent on the power, as indicated in the Observations from **Section 3.0.1**) is most probably inhibiting the heat from the laser beam from spreading into the underlying microcellular structure. As this melted surface layer increases in thickness, lesser energy is transferred to the microstructure, consequently leading to lesser growth/nucleation from individual bubbles.

Chapter 4.0 Energy and Temperature Considerations

4.1 Energy delivered to the specimen by the laser beam

The speed and power settings of the laser beam inducing foaming in the specimen eventually influence or contribute to one important quantity that dictates whether the specimen successfully or partially foams, or gets burnt, and that is the energy delivered to the specimen. Therefore, an area of focus in this study is to determine a value for the energy that is given to a specimen, from the input settings applied.

Here are some of the known quantities to start off the calculations for energy:

- Power (in W) = $\frac{\mathrm{p}}{100}$ * 40
- Speed (in m/s) = $\frac{v}{100}$ * 82 * 0.0254
- All specimens had a nominal thickness of 1.5 mm,

  Sample Height = $1.5 * 10^{-3}$ m
- Taking a foamed area of 1.5 cm x 0.5 cm,

  Foam Area = $0.015 * 0.005 = 7.5 * 10^{-5}$ m^2
- DPI = 1200

Calculated quantities:

From the DPI setting we can find the dots per cm:

Dot cm^{-1} = 1200/2.54

The dots per cm^2 area can then be found as follows:

Dot cm^{-2} = (Dot cm^{-1}) * (Dot cm^{-1}) = **223200.45**

The total number of dots in the foamed patch of 1.5 cm x 0.5 cm:

Dot Total = Dot cm^{-2} * Foam Area (in cm^2) = ~**167,400**

The time taken per dot:

Dot Time (in seconds) = $\frac{Foaming\ Time}{Dot\ Total} = \frac{t_{foam}}{Dot\ Total}$

As the power is delivered per dot pulsed by the laser, we can find the energy delivered per dot:

Dot Energy (in J) = P * Dot Time

Total energy delivered to the specimen:

Total Energy (in J) = Dot Energy * Dot Total -------- (i)

Substituting values for the speed and power settings within the successful foaming process window (55% speed, 13% power and a foaming time of 23 seconds), yielded the following results:

- Time taken per dot: Dot Time = **$1.374*10^{-4}$ s**
- Energy delivered per dot: Dot Energy = **$7.145*10^{-4}$ J**
- Total energy delivered to the specimen: Total Energy = **119.6 J**

The energy delivered per dot and total energy delivered to the specimen are used in two separate approaches in the next two sections to estimate a surface temperature.

4.2 Surface Temperature estimation of specimens

Finding the energy value from the previous Section serves as a good initial stage to estimate a surface temperature reached by the specimen, so that we can understand at what temperatures laser induced foaming takes place. We can then better quantify this novel process, and this provides a standard of comparison with existing processes like the oil bath and hot press, where the temperature is an input variable.

In the following sections, two approaches to estimate the surface temperature are discussed.

4.2.1 Model 1 – Considering Energy per dot

In this approach the surface temperature is calculated using the energy per dot.

Let T = surface temperature and T_{inf} = ambient temperature

The energy supplied per dot causes a temperature rise in the specimen according to the following relation:

Dot Energy = $m*C_p * (T-T_{inf})$

Chosen values (PC properties taken from [15]):

T_{inf} = 23 °C, C_p = 1250 J/(kg·K), ρ = 1200 kg/m^3, spot size (diameter) = 0.1016 mm

m = vol. * ρ = $\frac{\pi}{4} * (0.1016 * 10^{-3})^2 * 670.0206 * 10^{-6} * 1200$

Some assumptions made using this model are:

- Circular spot size of 0.004 inches was considered, although the spot is elliptical with a major and minor diameter of 0.005 in and 0.003 in respectively.
- A depth till the transition region was considered when calculating the effective 'dot volume' foamed (see Fig). This was then used to find the mass quantity m when estimating the temperature.
- The temperature T being found is assumed to be the surface temperature, although the expression treats this as an overall, bulk temperature for the specimen.

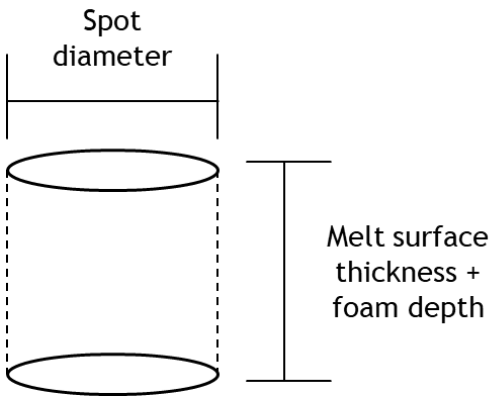

Figure 12: Effective 'dot volume' considered

Substituting the same values of speed, power and time as used in Section 4.1 (55% speed, 13% power and a foaming time of 23 seconds) we get,

Final predicted temperature **T = 110.69 °C**

This solution is lower than the expected range, since we know that the top surface has been melted by the laser from the SEM micrographs studied previously. The melting temperature of polycarbonate is in the approximate range of 220 °C – 260 °C [14], so a temperature in this vicinity should be expected.

4.2.2 Model 2 – Considering Total Energy delivered to the specimen and heat transfer losses

Another approach to estimating the surface temperature is considered here. This method uses the total energy delivered to the specimen (from equation (i) in Section 4.1).

Energy input = Energy causing temperature rise + Energy losses due to conduction, convection, and radiation -----(ii)

Chosen values (same as Model 1):

Ambient temperature = T_{inf} , Surface temperature = T

For energy causing temp rise: C_p = 1250 J/(kg·K), ρ = 1200 kg/m^3

Chosen parameters for conduction, convection, and radiation ([15]):

k = 0.22 W/(m·K), h = 0.21 W/(m^2K), ε = 0.94 and σ = 5.670367 * 10^{-8} W · m^{-2} · K^{-4}

Equation (2) can be written as:

Total Energy = m*Cp * (T-T_{inf}) + t_{foam} * (k*A*(T-T_{inf}) + h*A*(T-T_{inf}) + ε*A*σ*(T^4-T_{inf}^4)) ---- (iii)

As before, substituting 55% speed, 13% power and a foaming time of 23 seconds and using Python to solve the nonlinear equation (iii) for surface temperature T,

Final (predicted) surface temperature T = 519.1 ºC

This value, as opposed to model 1 was too high and exceeded a realistic range for the melting temperature of polycarbonate. A more refined approach may need to be considered to get an accurate representation of the surface temperature (see Section 5.2).

Some assumptions made using this model:

- To calculate the mass term in the energy causing temperature rise quantity (using volume * density), we considered a foam volume by taking the product of the area foamed by the specimen height and not by the melt surface thickness + foamed depth (used in model 1), because a smaller value for the volume causes the temperature rise to be even greater. So, to keep things simple, since we assumed a conduction loss for the surface in contact with the laser bed, the total specimen thickness was considered
- The temperature T being found is assumed to be the surface temperature, although the expression for '**Energy causing temperature rise**' treats this as an overall, bulk temperature for the specimen.

Chapter 5.0 Conclusions and Recommendations

5.1 Conclusions

In this study, the effect of speed and power of a laser beam was investigated on polycarbonate specimens saturated at different pressures of 1, 3 and 5 MPa. The results were delineated into two primary categories:

1. Graph plots of power vs. speed to help illuminate the process window for generating successful foams, based on a categorization of the appearance of the specimens after engraving by a laser beam. The visual spectrum of foamed engravings could be mainly isolated into three groups:
    a. Successful foams, which had a bright white appearance and were the main focus of this project
    b. Melted/burnt foams, which had a yellow, caramelized (or black) char on the engraved surface
    c. Partial foams, which had striped patterns or visible transparency in the engraved surface area
2. The successful foam microstructure for various specimens was investigated under the SEM, and the corresponding effect of varying the process parameters like speed, power, and saturation pressure on the micro scale features like melted (and resolidified) surface thickness, foam depth and average cell size was analyzed.

Some interesting results were obtained, some intuitive, while others were new inferences learned. A direct relation between speed and average cell size was established, as well as a limiting relation between power and average cell size, on account of the melted surface thickness inhibiting the heat from the laser beam. It was deduced that speed and power can be simplified into one intrinsic quantity that is energy, and an attempt was made to estimate this energy delivered by the laser beam and the consequent temperature rise at the surface of the specimen.

The feasibility and impressive control given to the user has also been successfully demonstrated using this new technology to selectively induce nucleation where desired. Various intricate patterns foamed using a laser beam, which would be impossible to achieve using the current processes like the oil bath and hot press, have been depicted in **Figure 13** on the next page.

*Figure 13: (Clockwise from top left): **13a**: A geometric pattern of foamed concentric circles. **13b**: Custom text can be written using this technique. **13c**: University of Washington insignia.*

5.2 Recommendations for future work

This study has paved the way for a lot of exciting new avenues and possibilities for using lasers to selectively foam polymers. Some shorter term enhancements to the current work, as well as longer term exploratory investigations are suggested and discussed.

5.2.1 Near-term ideas

The results obtained in Section 3.2 can be refined by taking micrographs at the same magnifications and re computing an average cell size to ensure uniformity in raw data.

The results in Section 3.3 can similarly be refined by choosing a region of cells at a fixed distance from the melted surface thickness, for different power settings, all other factors remaining constant.

5.2.2 Longer term research ideas

Some ideas for long term future work could involve:

Varying the thickness of specimens to be engraved, as this changes the CO_2 concentration at equilibrium, and could therefore lead to different micrographs, i.e. potentially altered cell sizes and corresponding foam depth.

Calculating the cell nucleation density achieved by this new method. This could be used to find a measure of the relative density of foamed structures that lasers have the capability of producing. This has promising applications in sustainable development, specifically for weight reduction and material conservation, in situations where material strength is not a critical factor.

Laser induced foaming can also be investigated on other polymer materials, where different properties may be created, leading to different potential applications. This novel technique has proven to be versatile enough to work with PEI, by performing a few preliminary experiments where we were able to obtain a successful foam (**Figures 14a, 14d** and **Figure 15**).

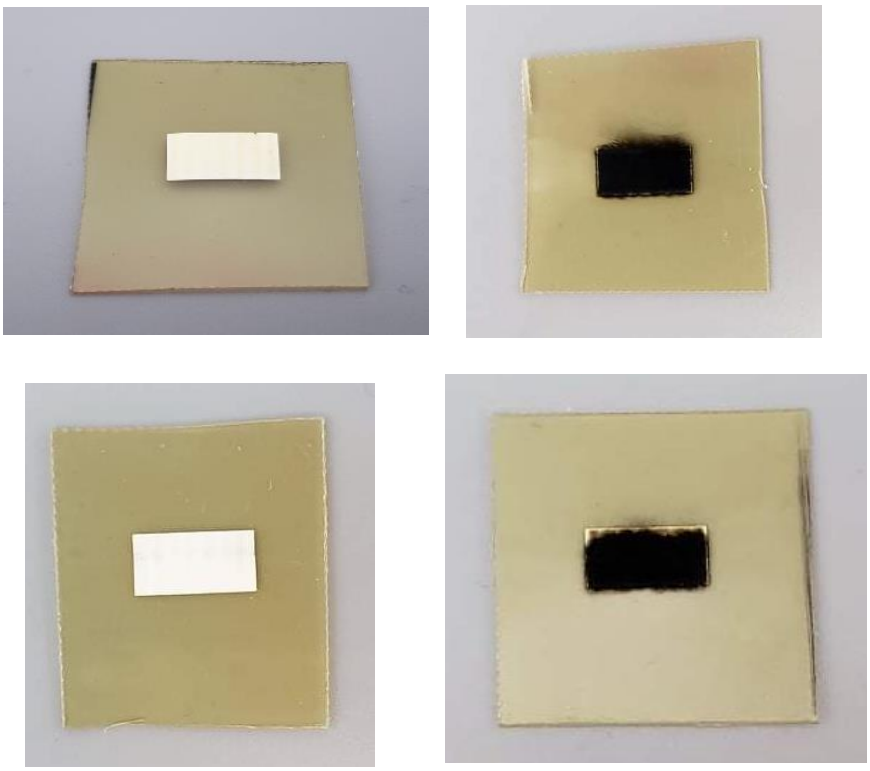

Figure 14: (Clockwise from top left) ***14a****: This specimen was foamed at 23% speed and 7% power settings. The foam appears to have a slight yellow tint, and some faint lines from the laser pattern can be observed.* ***14b****: This was foamed at 23% speed and 9% power settings. The specimen is completely burnt, after only a 2% power increase. We then decided to decrease the power by 1% for* ***14c*** *(bottom right), which was foamed at: 23% speed and 8% power. What was very surprising was the sharp change in foam quality from successful foam in* ***14a*** *to completely burnt in* ***14c****, despite having a very minimal power increase. The yellowed edges at the top of the specimen can be observed and indicate that the foam initially started off in the melted phase, but then immediately got burnt.* ***14d*** *(bottom left) was foamed at 20% speed and 5% power settings which yielded a bright white foam, which is again an intriguing result, since it was expected that PEI foams might retain a yellow tint, on account of the polymer's natural color. However, this was an identical looking foam to the ones achieved using polycarbonate.*

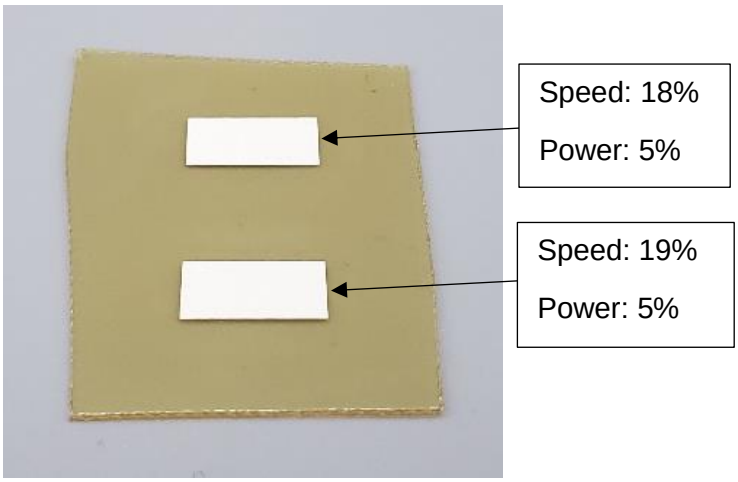

Figure 15: We were able to obtain bright white foams once again in this specimen, at the settings shown above.

It would also be prudent to explore the range of bubble sizes that can be achieved by altering the dots per inch (DPI) setting and studying how this affects the overall microstructure. We created 3 foamed patches at settings of 600, 400 and 200 DPI (**Figure 16**).

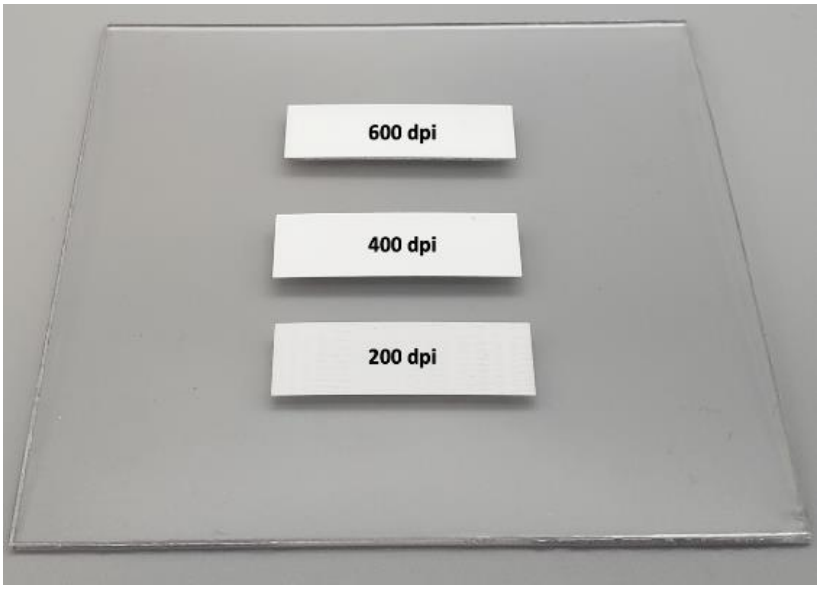

Figure 16: Different DPI settings foamed on one specimen

An interesting observation was that the foamed patches get progressively smoother to the touch as the DPI setting is decreased. A relation could be established in the microcellular range, of DPI vs. melted layer thickness, and how this corresponds to the surface roughness, which could be measured using a profilometer. Further possible relationships could be explored between the DPI

setting and how or if this influences the average bubble size, as well as the energy (keeping speed and power constant) and subsequently the surface temperature of the specimen.

Finally, regarding the surface temperature estimation models, the obtained values were likely inaccurate due to applying the $mC_p * \Delta T$ expression for a point source laser beam that is continuously moving. Thus, as the laser is a pulsed source that traverses along the polymer surface with time, it would be ideal to develop an FEM based approach with a governing equation (possibly based on laser welding analytical expressions) to determine a predicted temperature distribution along the surface, for future. This model should also be ideally validated with real temperature data measured for various settings of speed and power, by using temperature measurement devices, like a thermocouple or a thermal camera.

Chapter 6.0 References

1. J. Martini, F.A. Waldman and N.P. Suh, *Proceedings of SPE Antec 82,* San Francisco, CA, USA, 1982, 674.
2. J.E. Martini-Vvedensky, N.P. Suh, and F.A. Waldman, inventors; Massachusetts Institute of Technology, assignee; US 4,473,665, 1984.
3. V. Kumar and J.E. Weller, *International Polymer Processing*, 1993, **8**, 1, 73.
4. V. Kumar and J.E. Weller, *Journal of Engineering for Industry*, 1994, **116**, 11, 413.
5. R. E. Murray, J.E. Weller and V. Kumar, *Cellular Polymers*, 2000, **19**, 6, 413.
6. V. Kumar, and O.S. Gebizlioglu, *Proceedings of SPE Antec 92*, Detroit, MI, USA, 1992, 1536.
7. Y.P. Handa, B. Wong, Z. Zhang, V. Kumar, S. Eddy and K. Khemani, *Polymer Engineering and Science*, 1999, **39**, 1, 55.
8. V. Kumar, R.P. Juntunen and C. Barlow, *Cellular Polymers*, 2000, **19**, 1, 25.
9. H. Guo, A. Nicolae, V. Kumar. Solid-state microcellular and nanocellular polysulfone foams. *Journal of Polymer Science, Part B: Polymer Physics* 2015, 53, 975-985. (featured in journal cover)
10. H. Guo, V. Kumar. Solid-state PMMA nanofoams. Part I: low-temperature CO_2 sorption, diffusion, and the depression in PMMA glass transition, *Polymer* 2015, 57, 157-163.
11. H. Guo, V. Kumar. Some thermodynamic and kinetic low-temperature properties of the PC-CO_2 system and morphological characteristics of solid-state PC nanofoams produced with liquid CO_2. *Polymer* 2015, 56,46-56.
12. Y. Paul Handa and Zhiyi Zhang, Novel stress-induced nucleation and foaming process and its applications in making homogeneous foams, anisotropic foams, and multilayered foams, Cellular Polymers, Vol 19, January 2000.
13. John Weller, *The effects of processing and microstructure on the tensile behavior of microcellular foams (1996)*, page 24.
14. Polycarbonate Data Sheet, Chapter 4: Thermal Properties, Section 4.1.2 Melting Point, page 3 [Online]. Available: https://www.m-ep.co.jp/en/pdf/product/iupi_nova/physicality_04.pdf. [Accessed Dec. 8, 2021]
15. "Handbook for Producers of Plastic Raw Materials... (bistra.com.tr)", [Online]. Available: http://www.bistra.com.tr/eng_kdetay_print.asp?ha=126 [Accessed Aug. 5, 2021]

Appendix

This Section serves as a repository for various SEM micrographs taken for specimens foamed at different saturation pressures, speeds, and power settings in the laser engraver.

Additional foamed micrographs at 5 MPa:

After fracturing the samples which had successfully foamed in liquid nitrogen, they were imaged under a Scanning Electron Microscope (SEM). The following micrographs were obtained for these foamed specimens (the speed and power settings are mentioned above the batch of Figures).

(Specimen number - Date foamed)
S2 – 1/30 (**status**: successfully foamed):
Speed: 23% **Power:** 7%

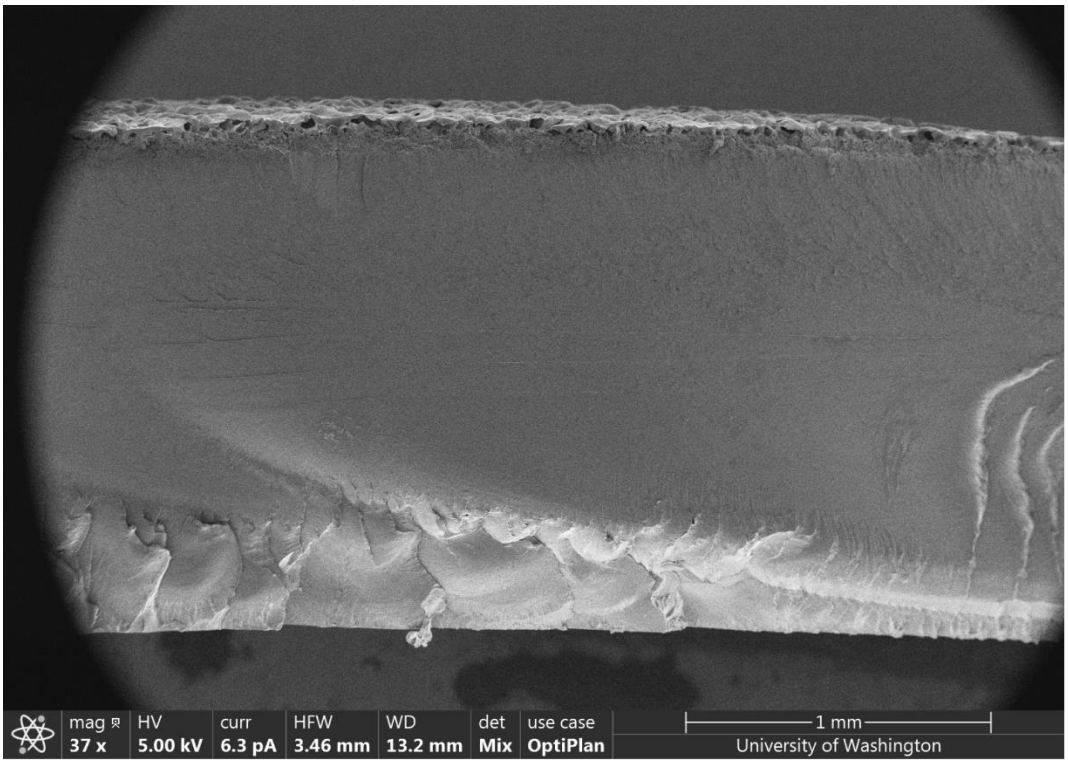

Figure A.17a: Full cross section thickness (foamed surface at the top of image)

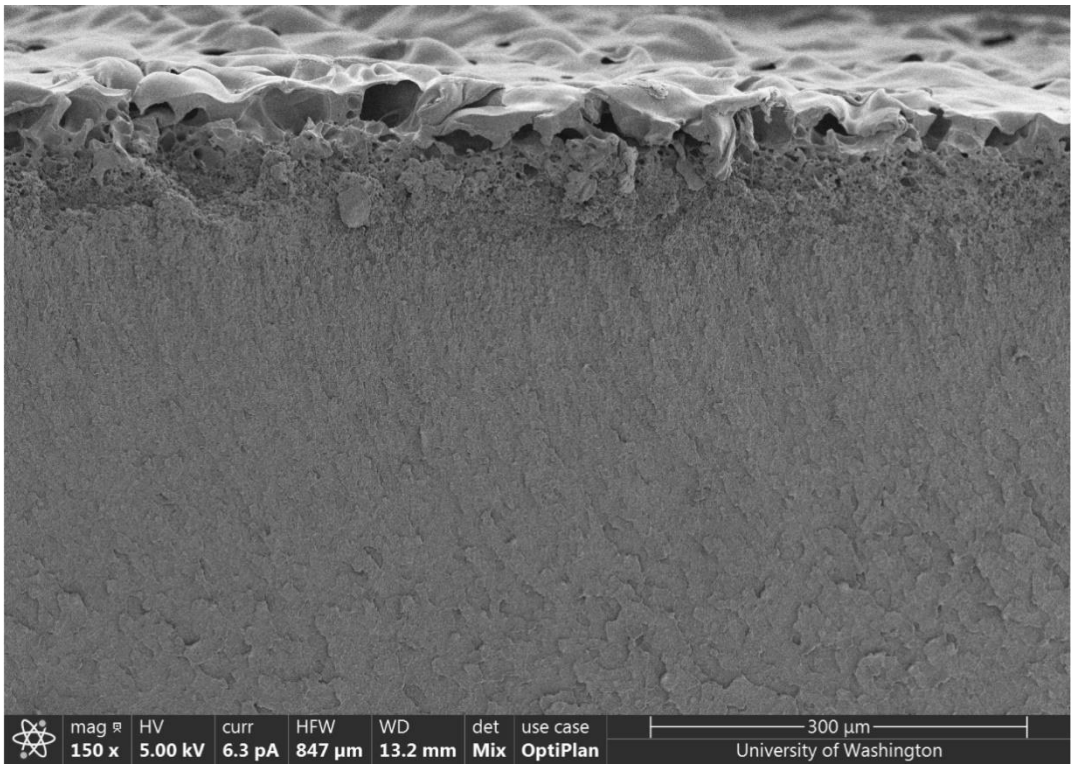

Figure A.17b: A closer look at the foamed surface. The bumpy surface indicates that it has been melted by the laser, and resolidified.

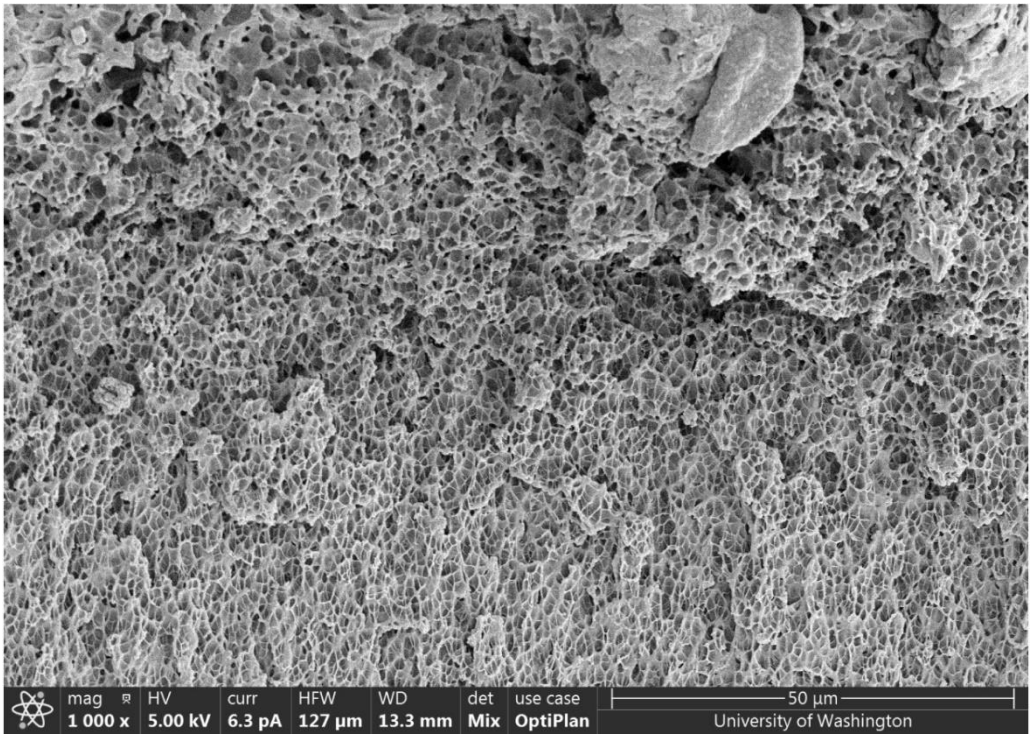

Figure A.17c: Foamed subsurface cross section magnified 1000x

S1 - 1/23 (**status**: successfully foamed):
Speed: 15% **Power:** 5%

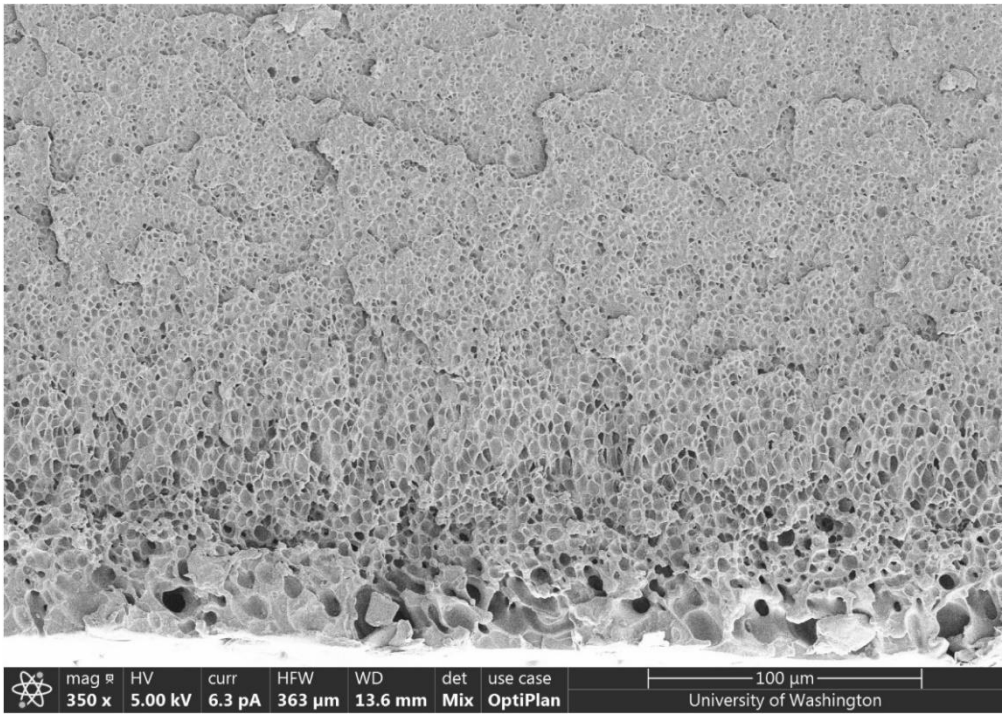

Figure A.18a: Foamed cross section thickness magnified 350x. The bubbles gradually decrease in size as we move away from the melted surface at the bottom of the image.

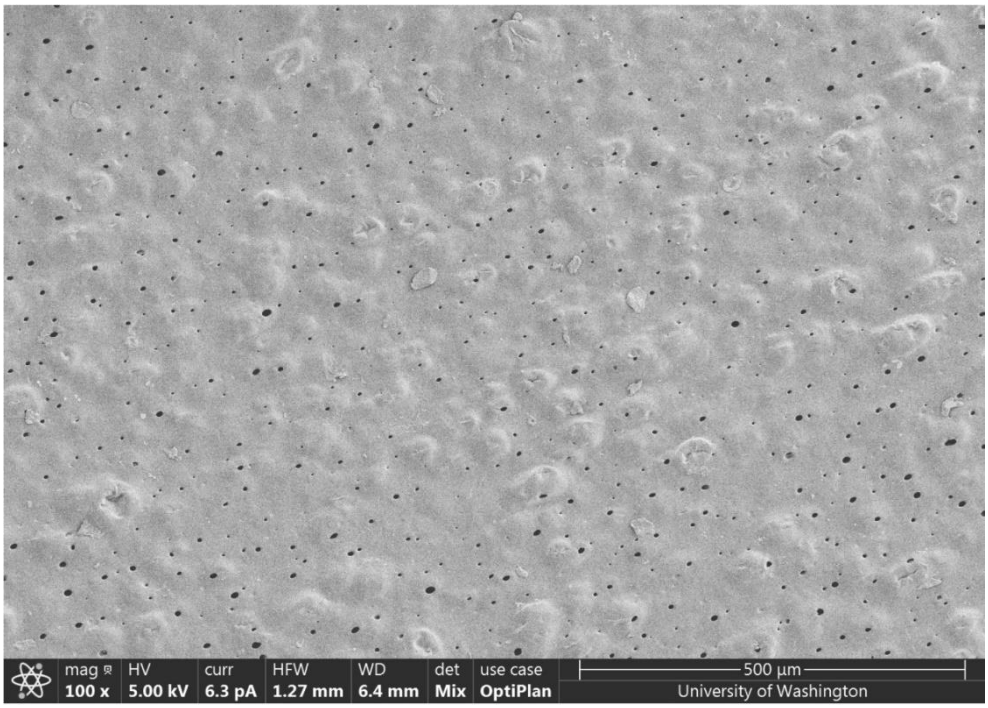

Figure A.18b: Foamed surface (top view) magnified 100x. A broader look at the same surface discussed in Chapter 3.0

S2 – 1/23 (**status**: successfully foamed):
Speed: 17% **Power:** 5%

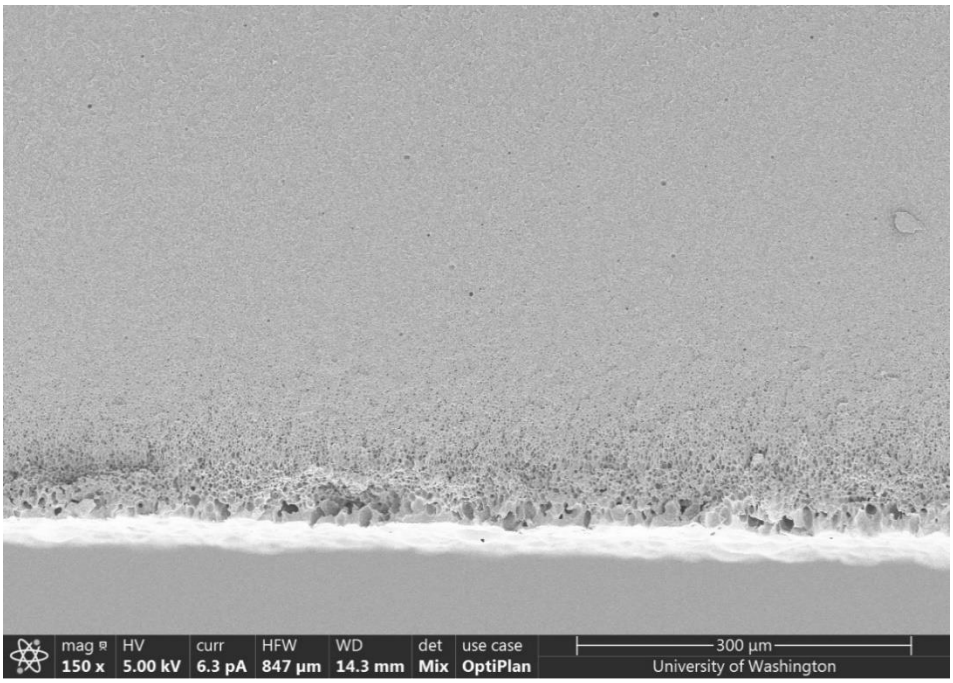

Figure A.19a: Foamed cross section thickness magnified 150x. We can already observe a fine distribution of microcellular bubbles from this distance

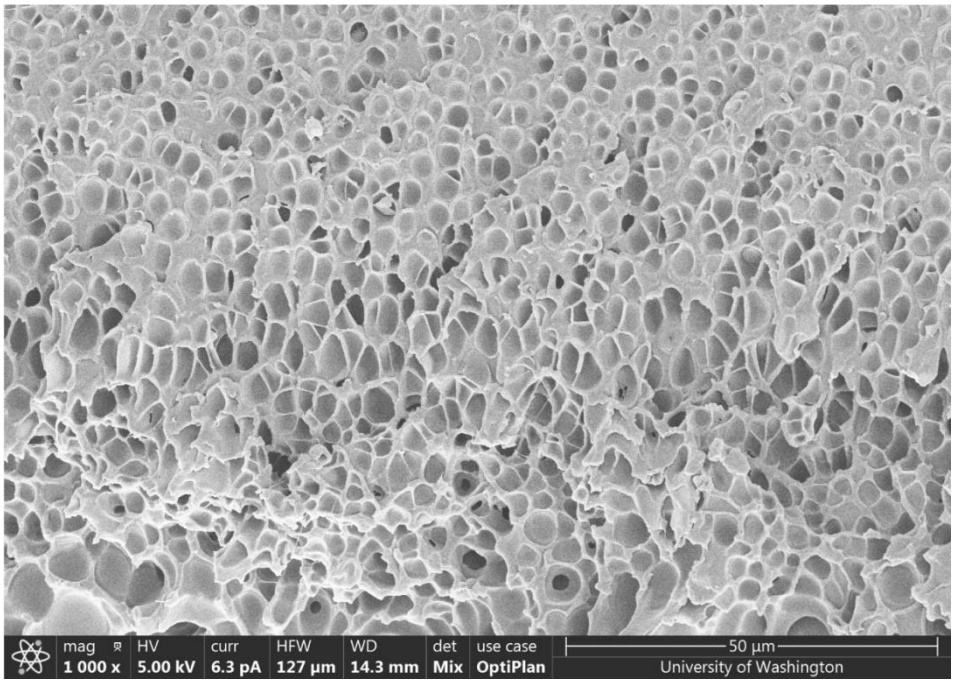

Figure A.19b: A closer look at the uniform cell distribution within the foamed cross section thickness.

S3 – 1/23 (**status**: successfully foamed):
Speed: 19% **Power:** 5%

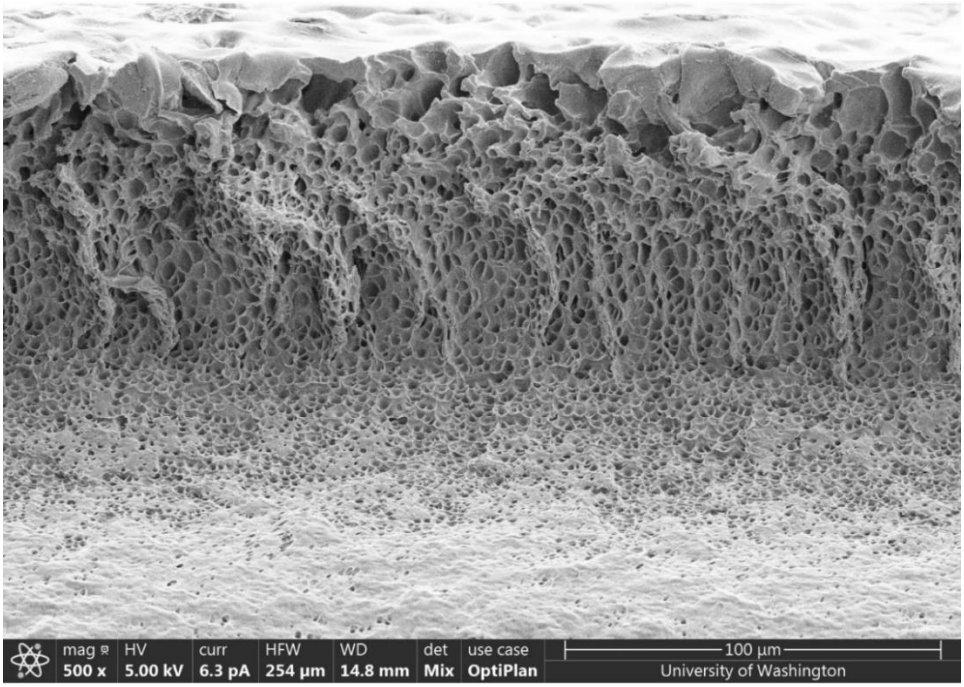

Figure A.20: Foamed cross section thickness magnified 500x. Microcellular bubbles visible under a melted surface layer.

S2 – 5/12 (**status**: successfully foamed):
Speed: 30% **Power:** 7%

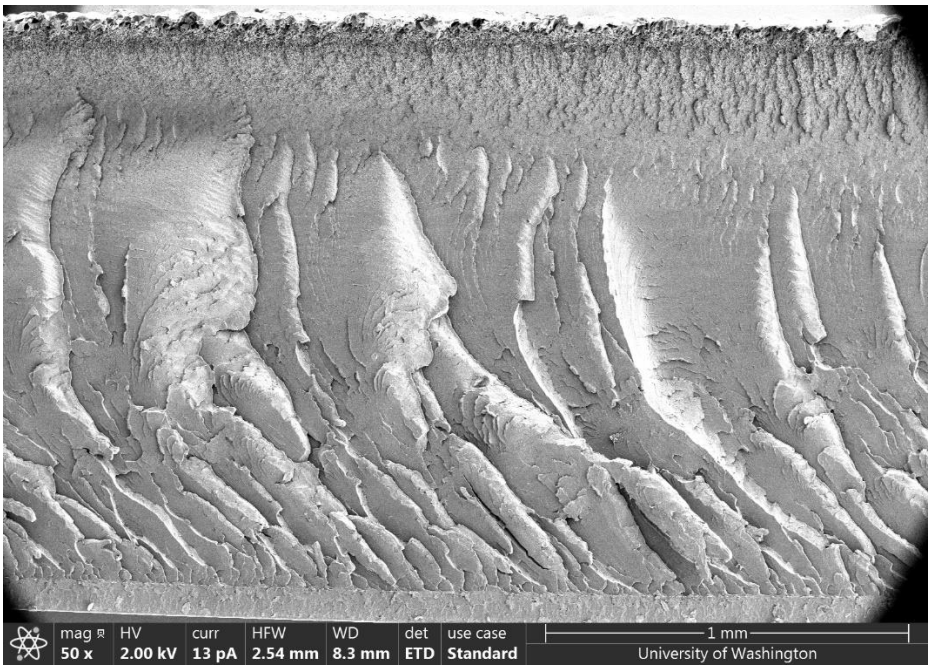

Figure A.21a: Full surface thickness depicting the microcellular structure near the top of the image, under the melted surface layer

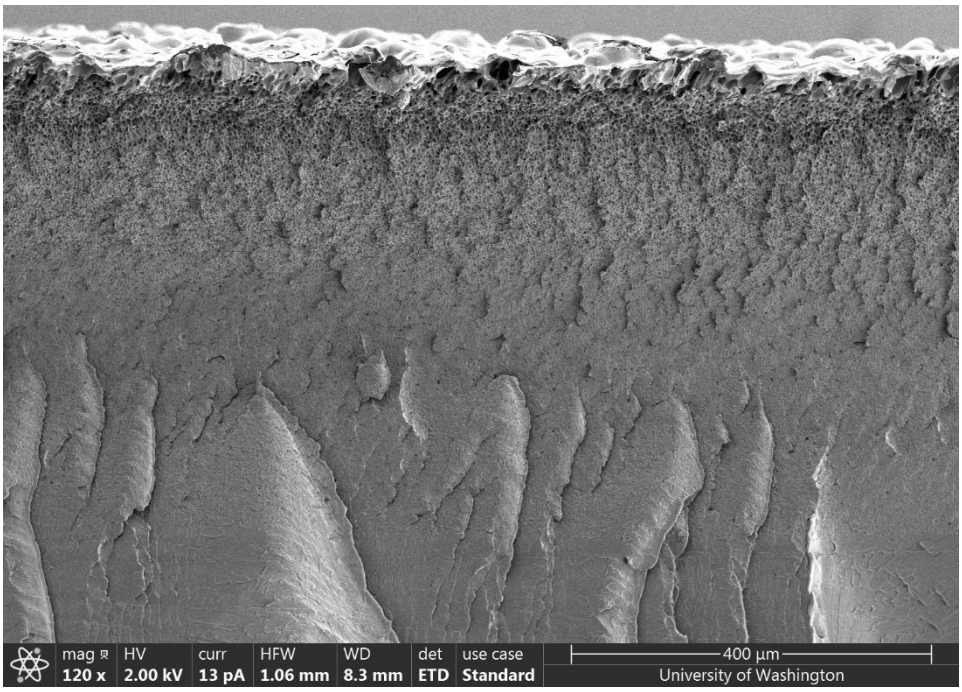

Figure A.21b: A closer look at the structure near the surface of the specimen

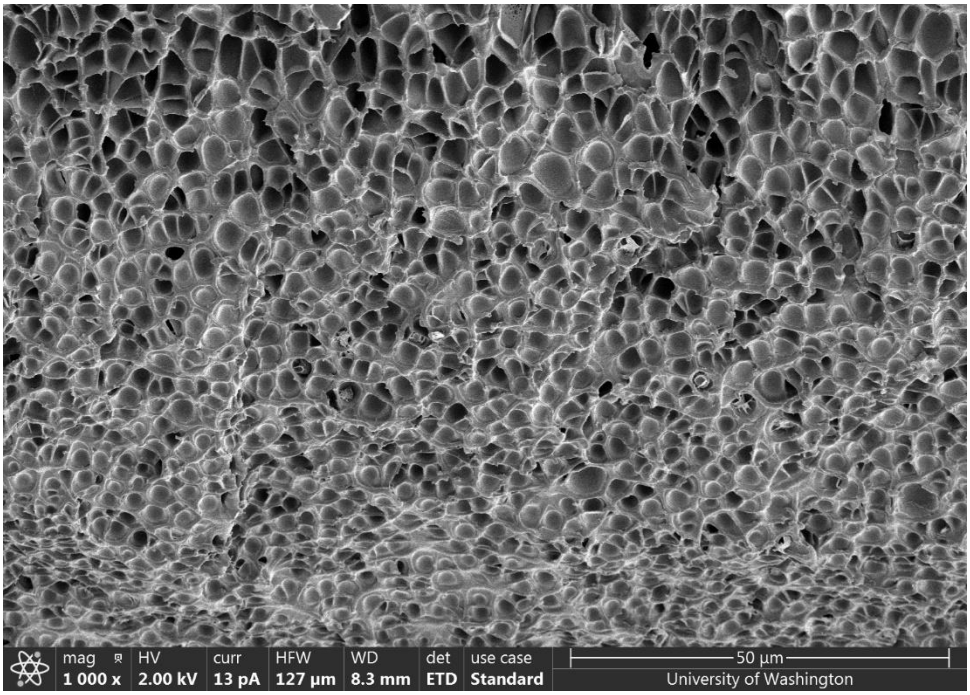

Figure A.21c: A fine, honeycomb structure of cells observed at 1000x. Even in this compact region, we can see a gradual shift in cell geometry from elliptical to circular as we go down the micrograph

S4 – 5/12 (**status**: successfully foamed):
Speed: 35% **Power:** 8%

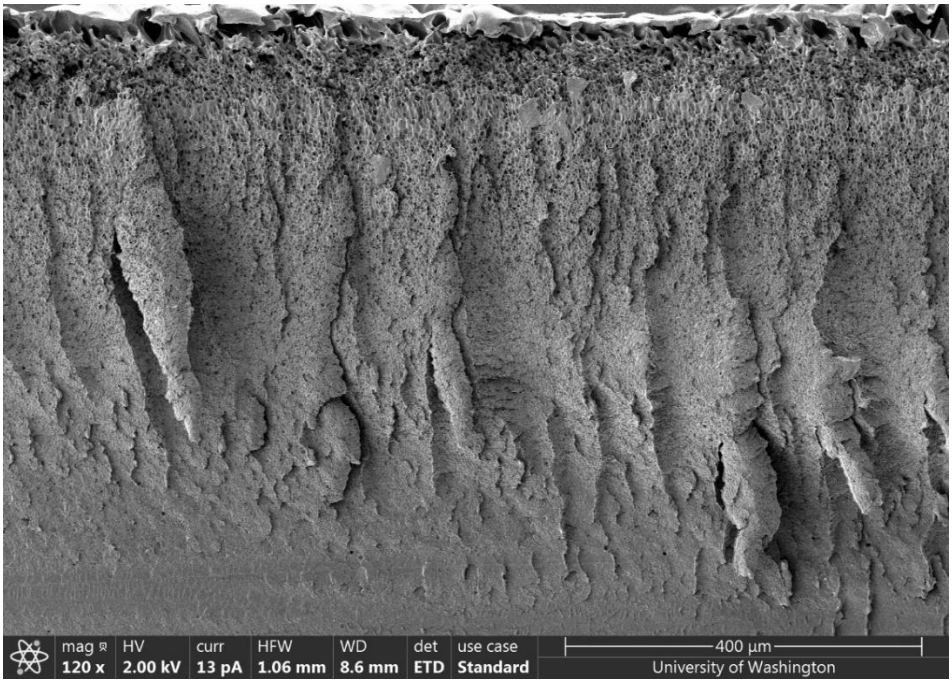

Figure A.22a: Cells near the melted surface layer (at the top of the image) are gradually decreasing in size while increasing in circularity as we move away

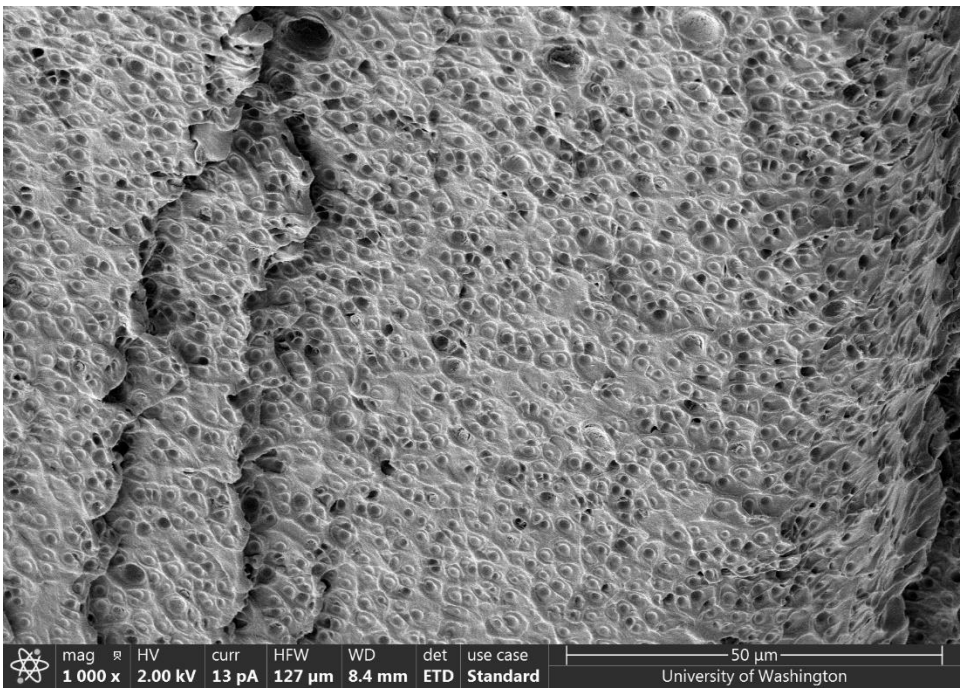

Figure A.22b: Cells near the transition region from microcellular to solid PC. These cells appear to be a lot less pronounced in definition compared to cells in the uniform cell region in other foamed specimen SEM images

Additional foamed micrographs at 3 MPa:

(Specimen number - Date foamed)

S1 – 4/21 (**status**: successfully foamed):

Speed: 13%, Power: 5%

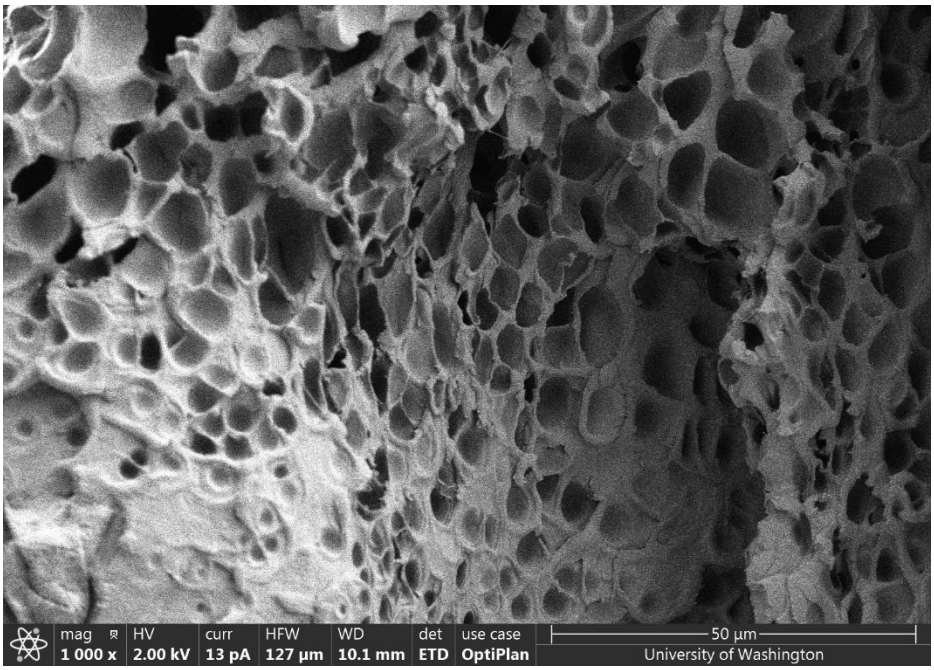

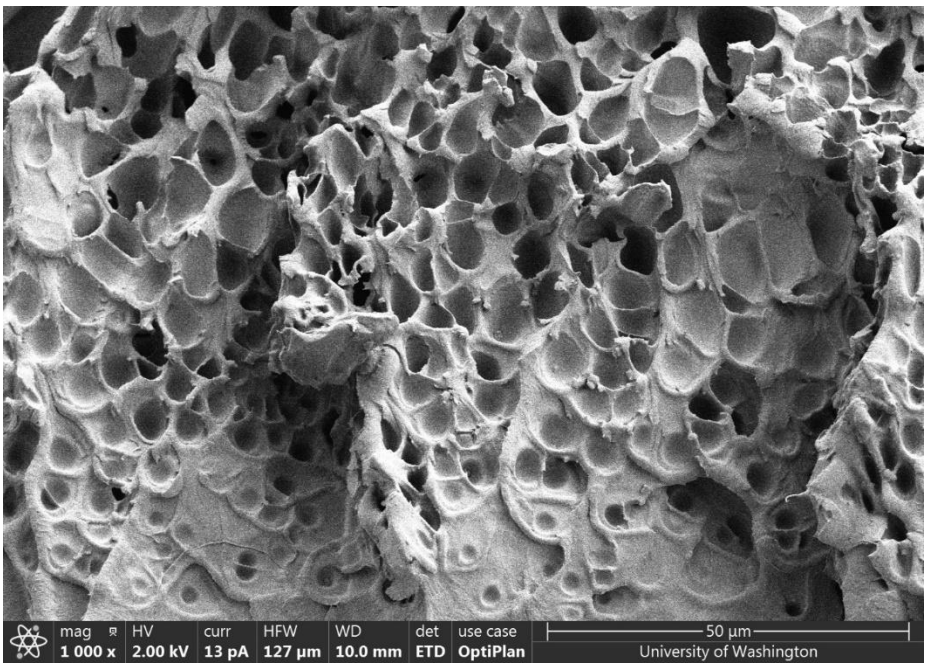

Figure A.23: Different locations in the micrograph are imaged at the same magnification. Bubbles appear to be distorted due to the manner in which the specimen was fractured.

S3 4-21 (**status**: successfully foamed):

Speed: 20%, Power: 7%

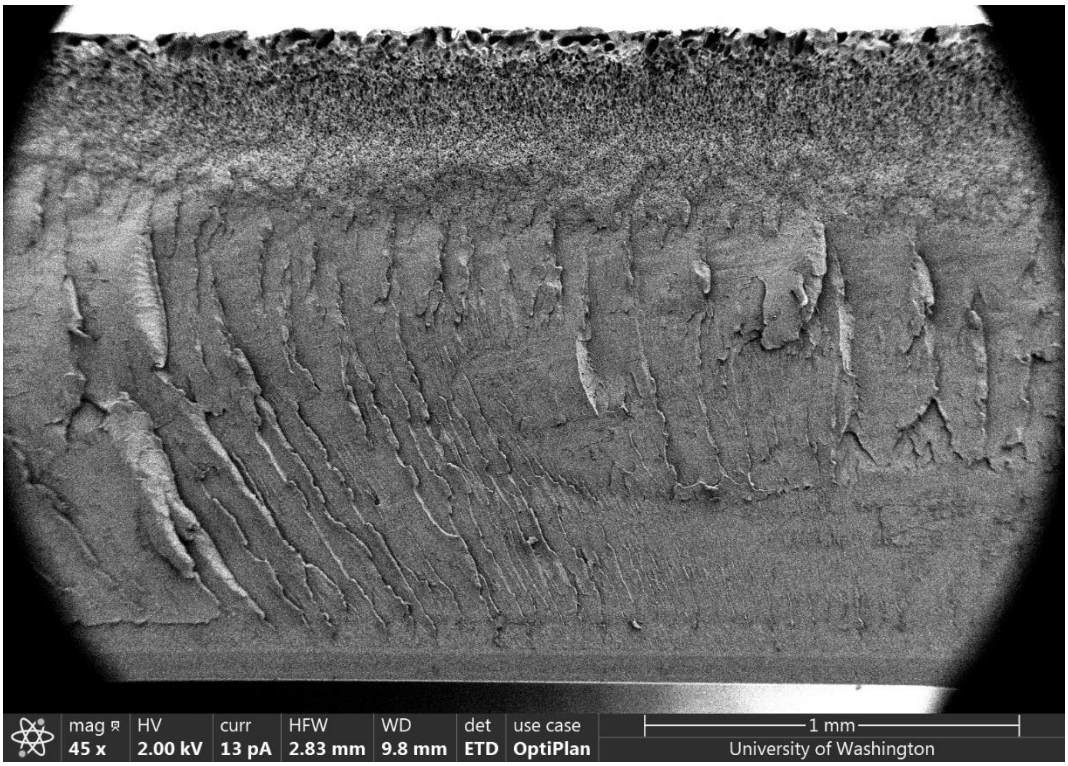

Figure A.24a: Full thickness micrograph. The foamed side is at the top of the image.

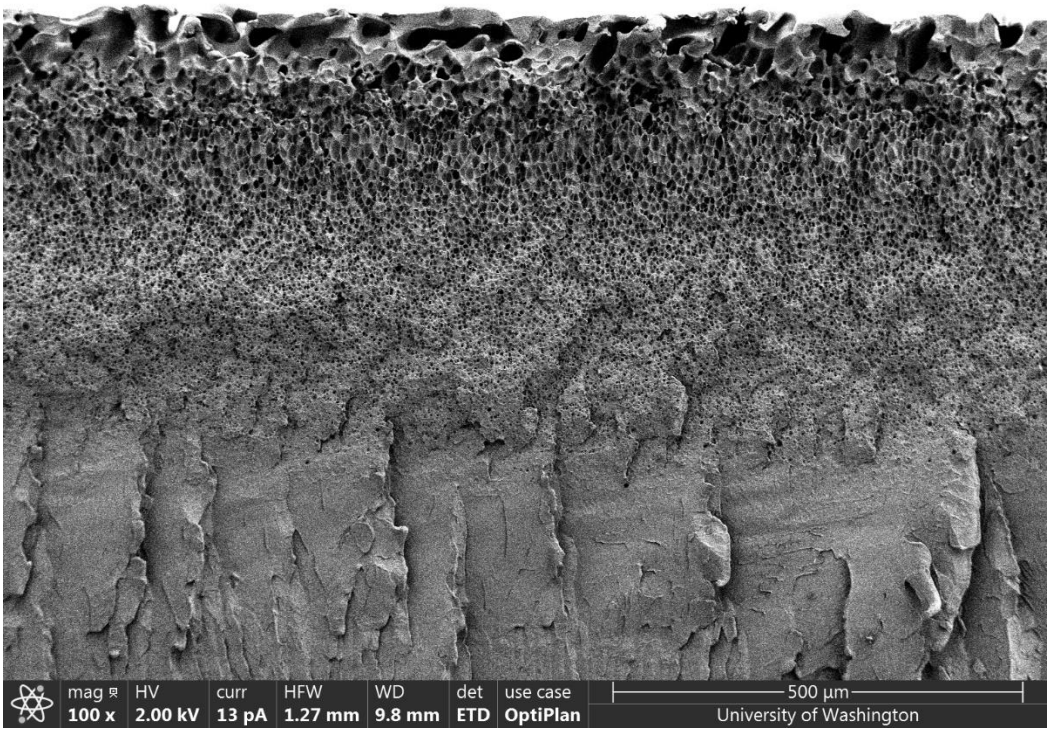

Figure A.24b.:A closer look at the foamed side of the cross section

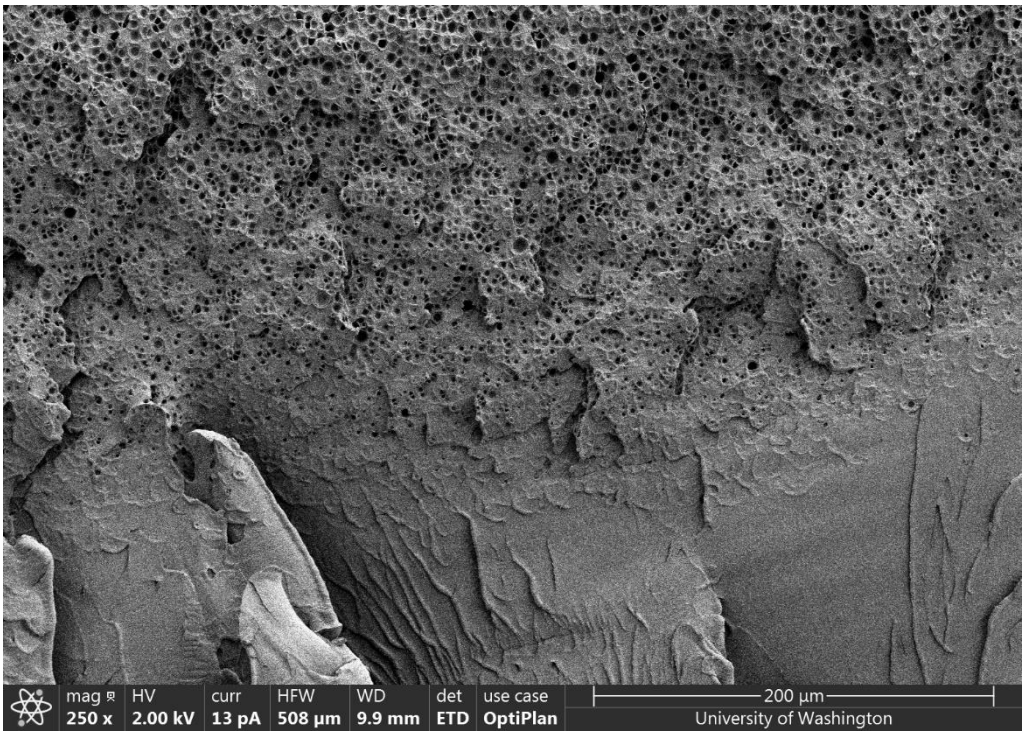

Figure A.24c: The cell structure appears to be very circular from a distance. The cell distribution also gradually decreases in density and cell size until the solid PC structure (end of foam) is reached.

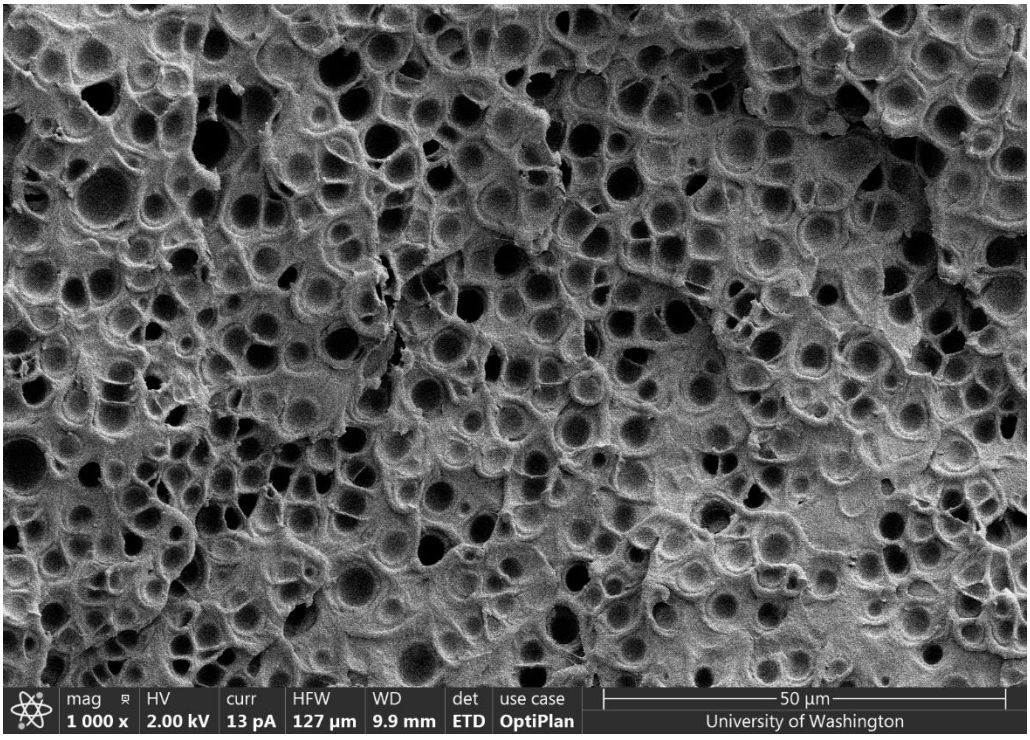

Figure A.24d: A closer look at the uniformly foamed microstructure reveals that the cells are indeed quite circular. The cell size appears to range between 2-4 microns.

S4 4-21 (**status**: successfully foamed):

Speed: 40%, Power: 10%

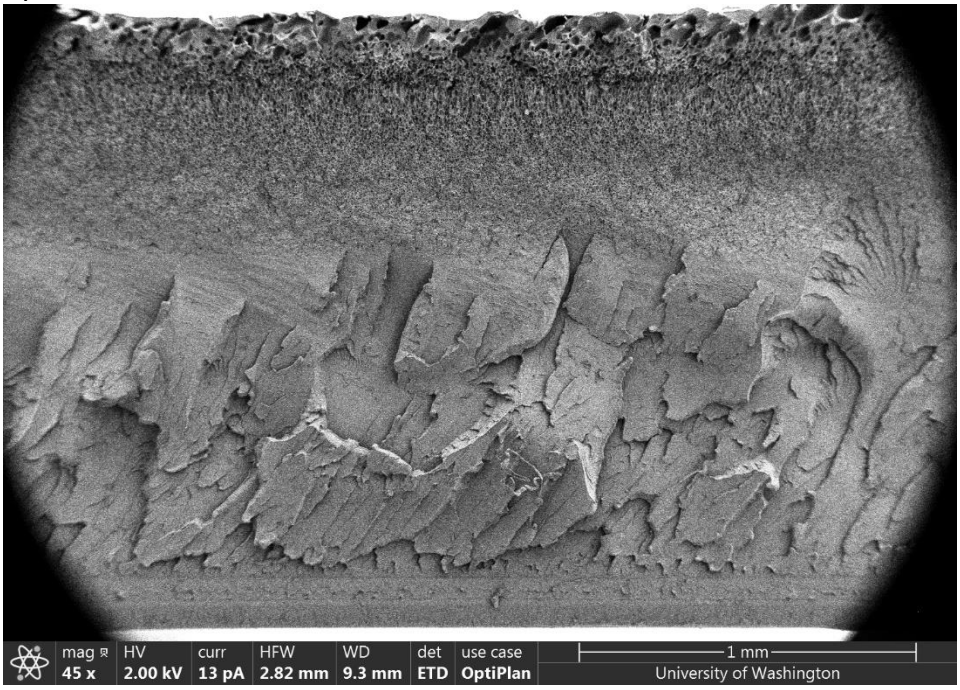

Figure A.25a: Full thickness depth of foamed PC. The upper surface has been exposed to the laser beam

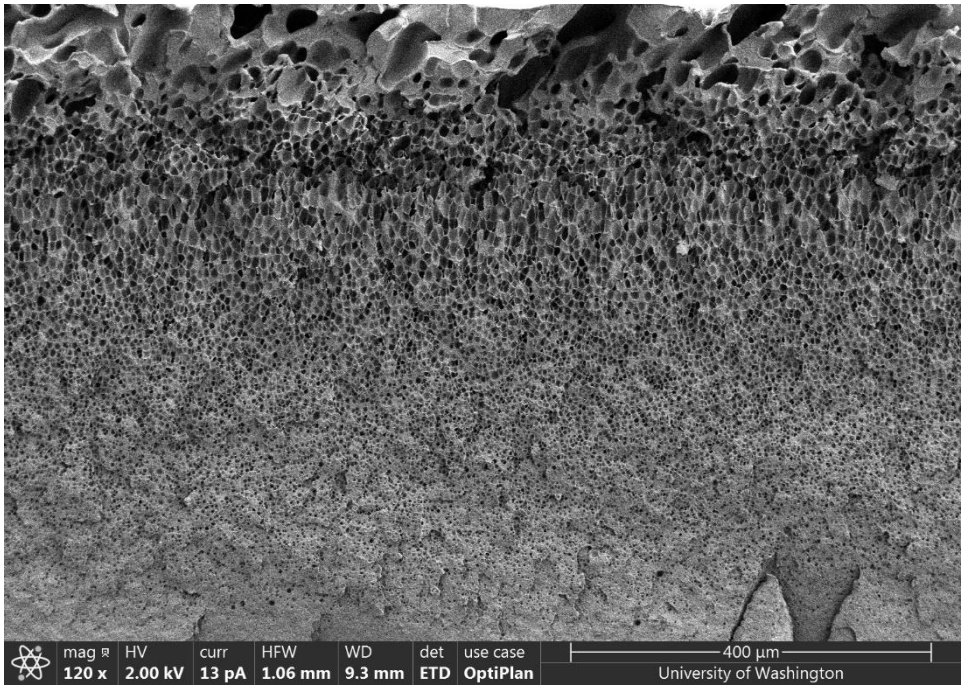

Figure A.25b: A closer look at the foamed side of the specimen reveals a honeycomb structure of closely grouped cells underneath the melted surface layer. The cells closer to the surface appear to be larger and more elongated, gradually becoming smaller and more circular as we move away from the melted surface layer, towards the bottom of the specimen.

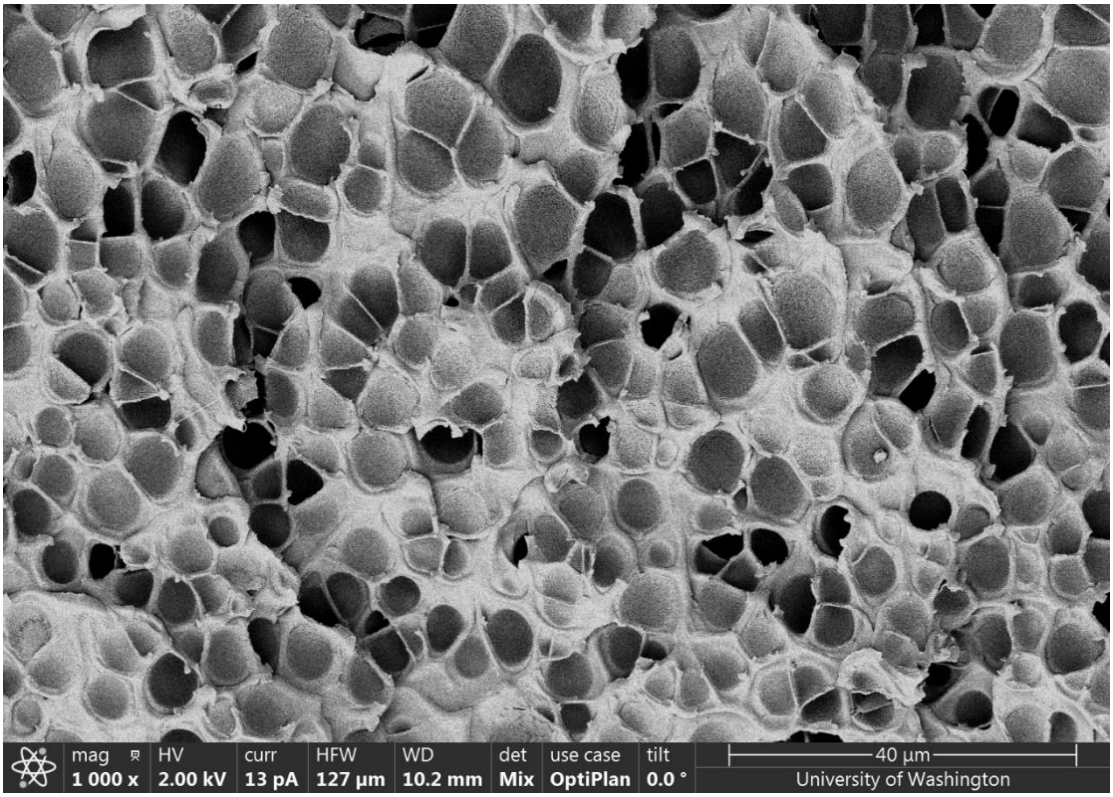

Figure A.25c: A magnified view of a section in the uniformly foamed region. These cells are also very similar in structure (circular) to the previous specimen. Once again, the cell sizes appear to range between 2-4 microns.

S5 4-21 (**status**: successfully foamed):

Speed: 55%, Power: 13%

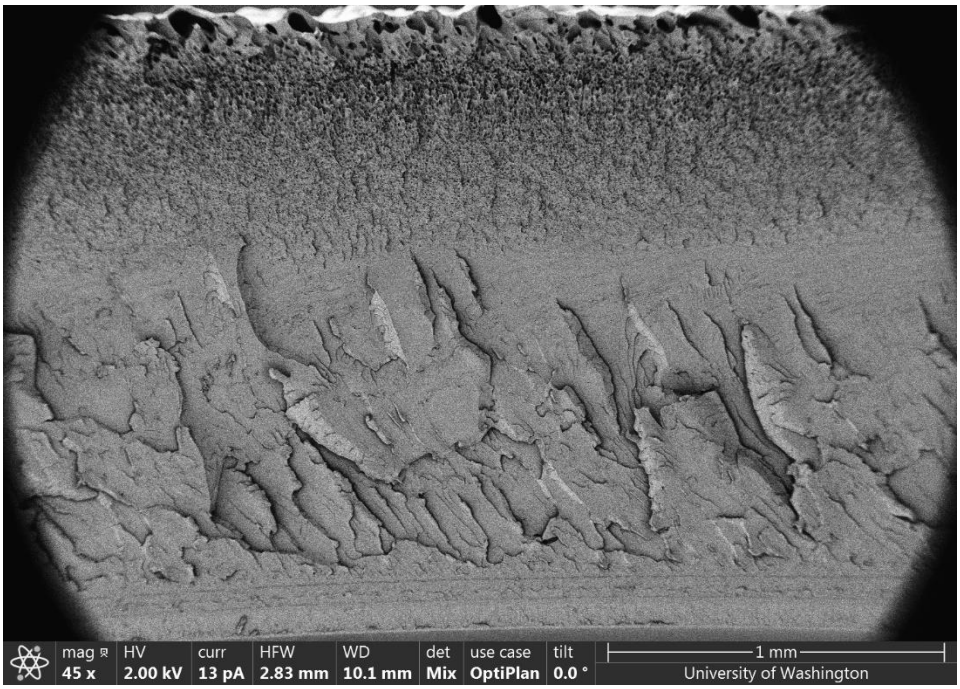

Figure A.26a: An overall perspective of the full thickness depth of the specimen. Artefacts from fracturing the specimen can be seen under the foamed layer

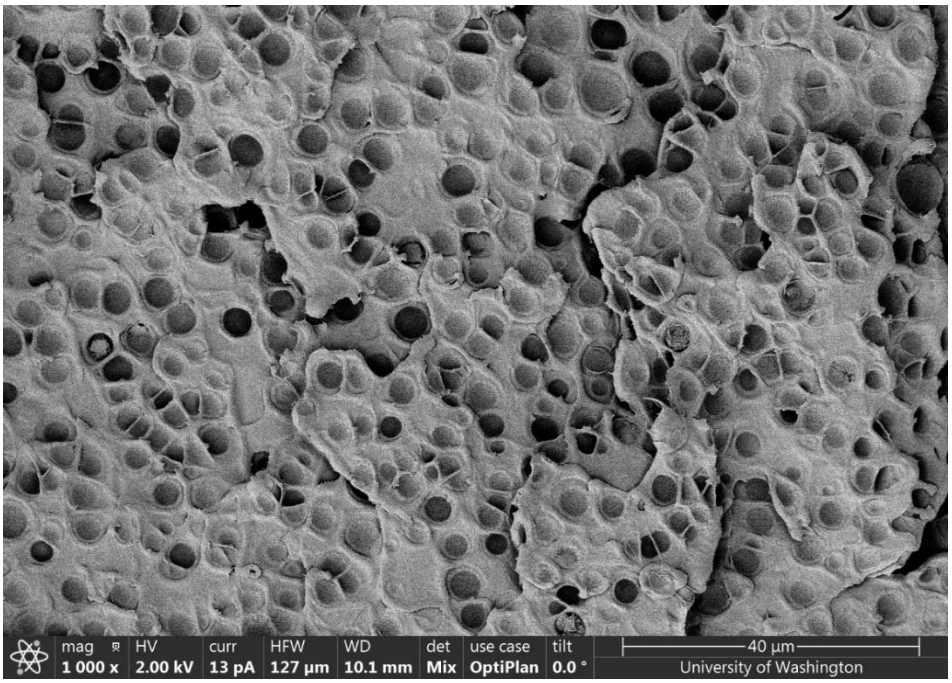

Figure A.26b: Once again we observe a very circular structure to the bubbles. The shape of the average cell may be directly determined by the saturation pressure, irrespective of speed and power within the foamed process window.

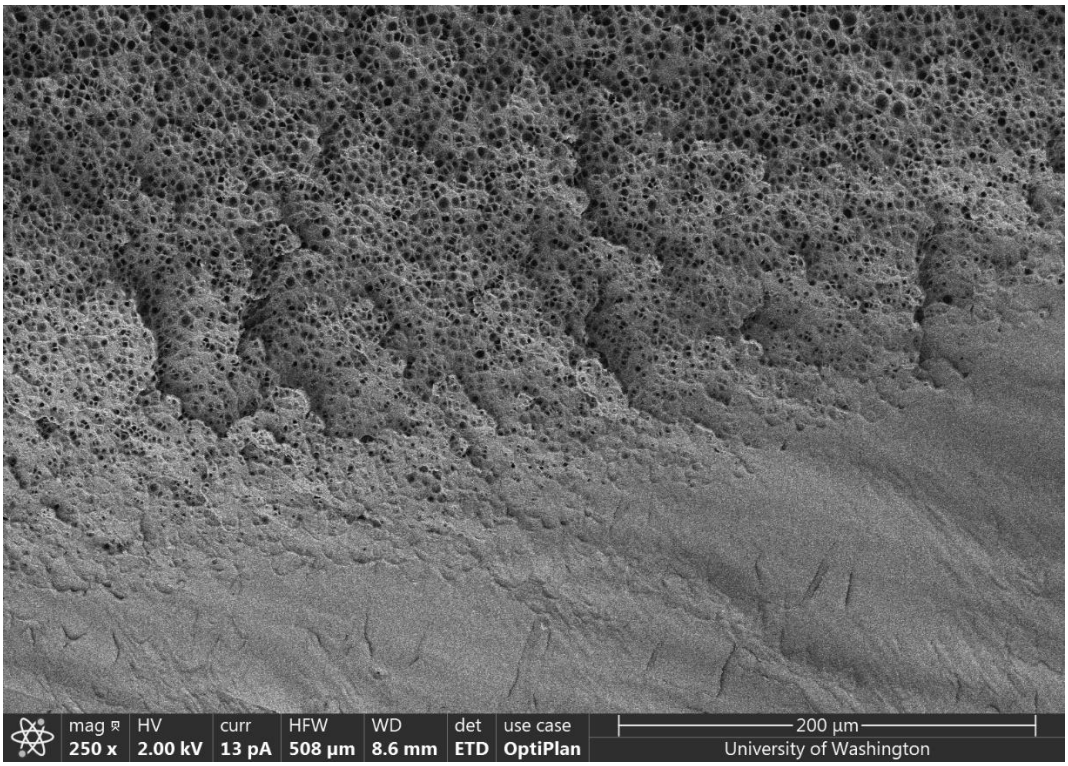

Figure A.26c: A distribution of circular cells can be seen gradually transitioning to a solid PC microstructure

Additional foamed micrographs at 1 MPa:
(Specimen number - Date foamed)
S3 - 4/28 (status: **successfully foamed**):

Speed: 20%, Power: 7%

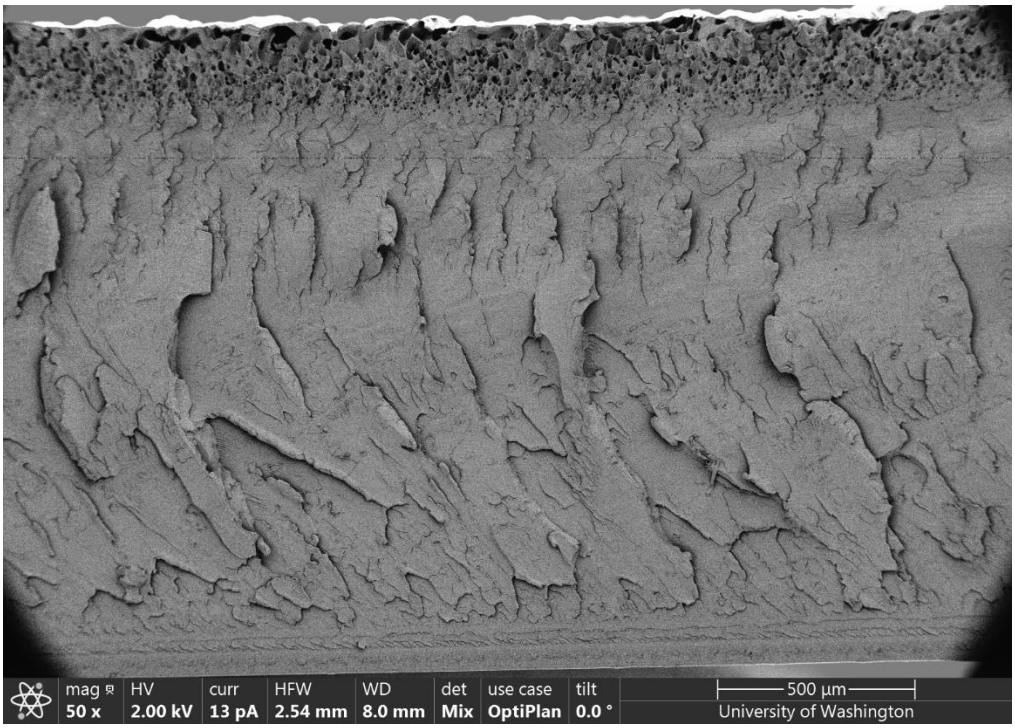

Figure A.27a: Full depth thickness of a fractured specimen. Most apparent is the stark difference in foam depth compared to the previous micrographs for the 3 MPa specimens

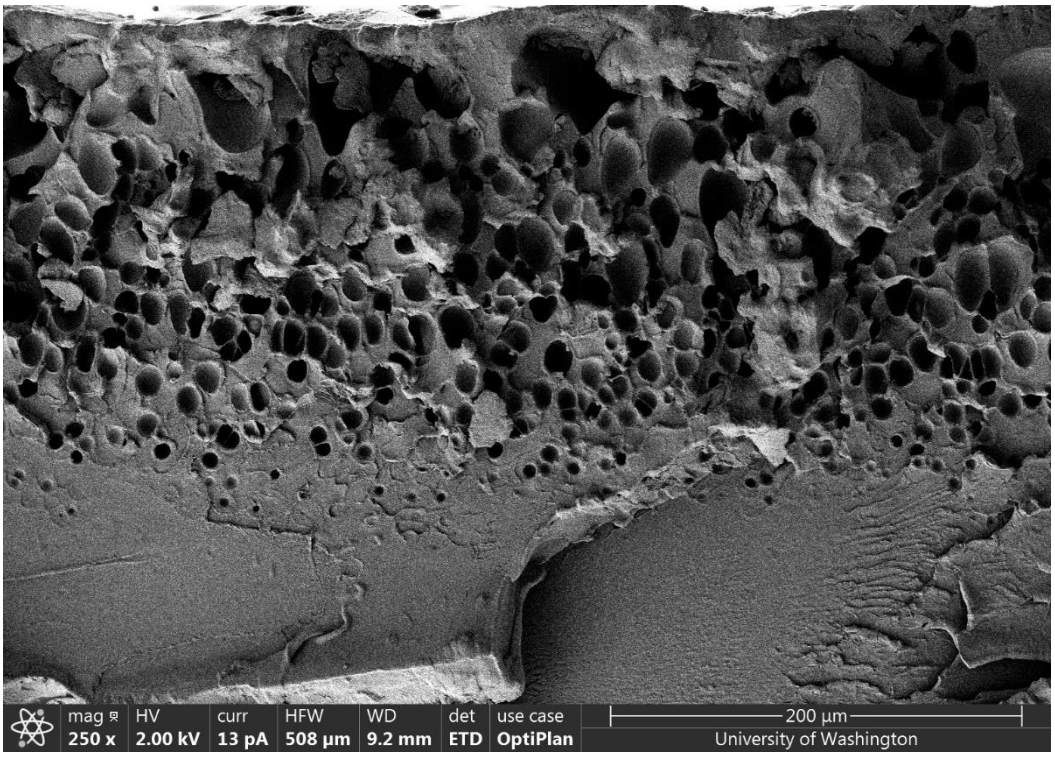

Figure A.27b: : A closer look at the bubble distribution. The cells are much larger, and not as uniform as the 3 MPa cells, and the foam rapidly transitions to solid PC

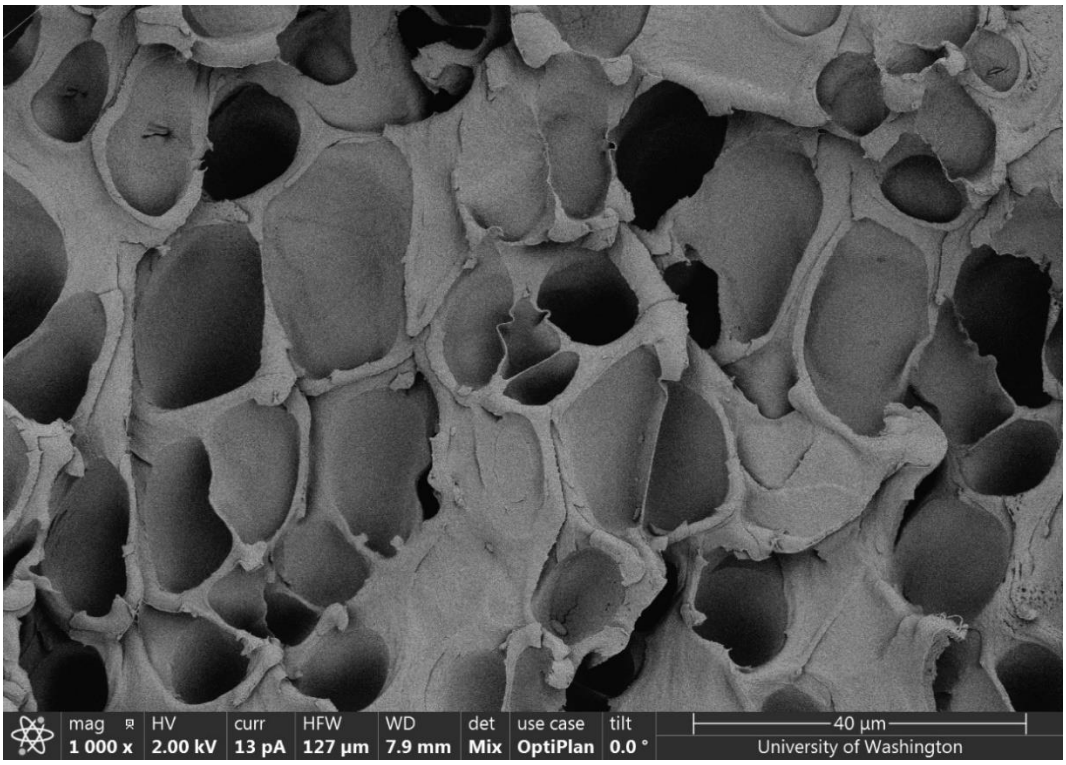

Figure A.27c: A closer look at the cells indicate just how large they are in comparison to the 3 MPa specimens. The cell size appears to range between 10 - 15 microns

S4 - 4/28 (status: **successfully foamed**):

Speed: 40%, Power: 10%

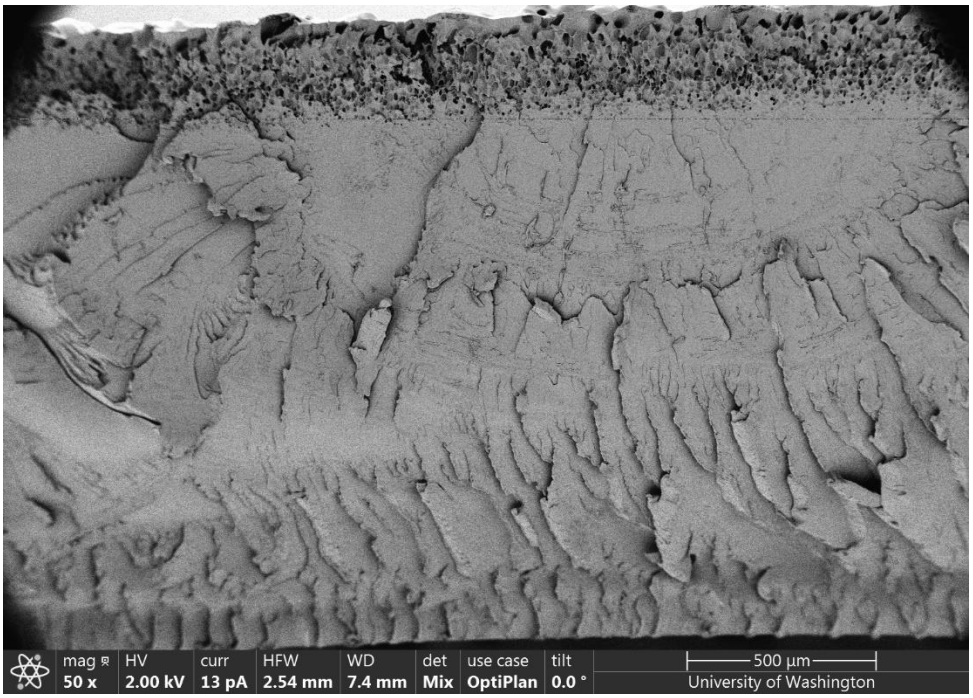

Figure A.28a: We observe a similar, shallow foam depth that was evident in the previous specimen. This indicates that there may be a limiting foam depth that can be achieved by specimens saturated at 1 MPa

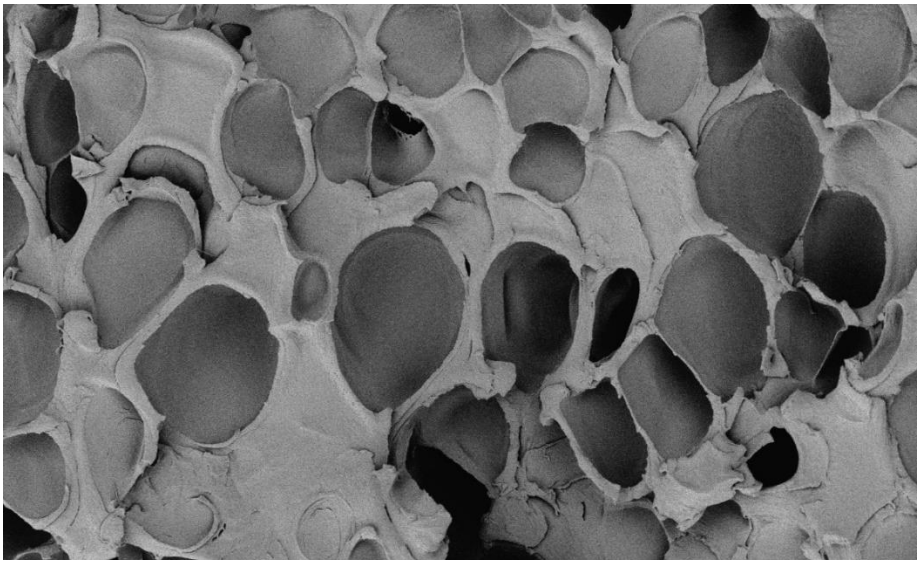

Figure A.28b: A closer look at the cells. These cells also seem to be of a similar scale, i.e. 10-15 microns

S5 – 4/28 (status: **successfully foamed**):

Speed: 55%, Power: 13%

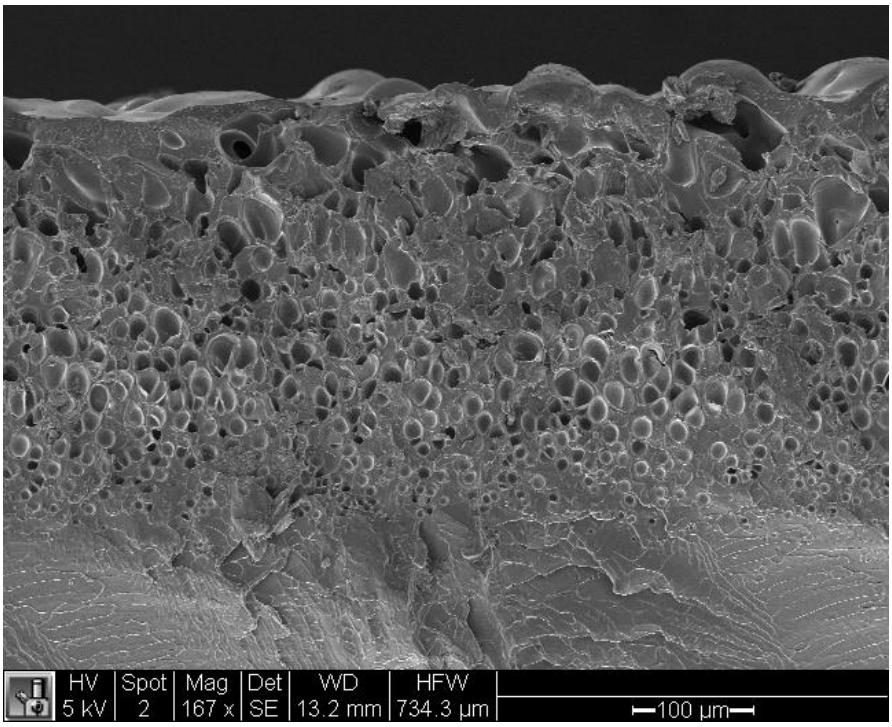

Figure A.29a: A magnified look at the foamed surface of the specimen. A different SEM was used to image these specimens.

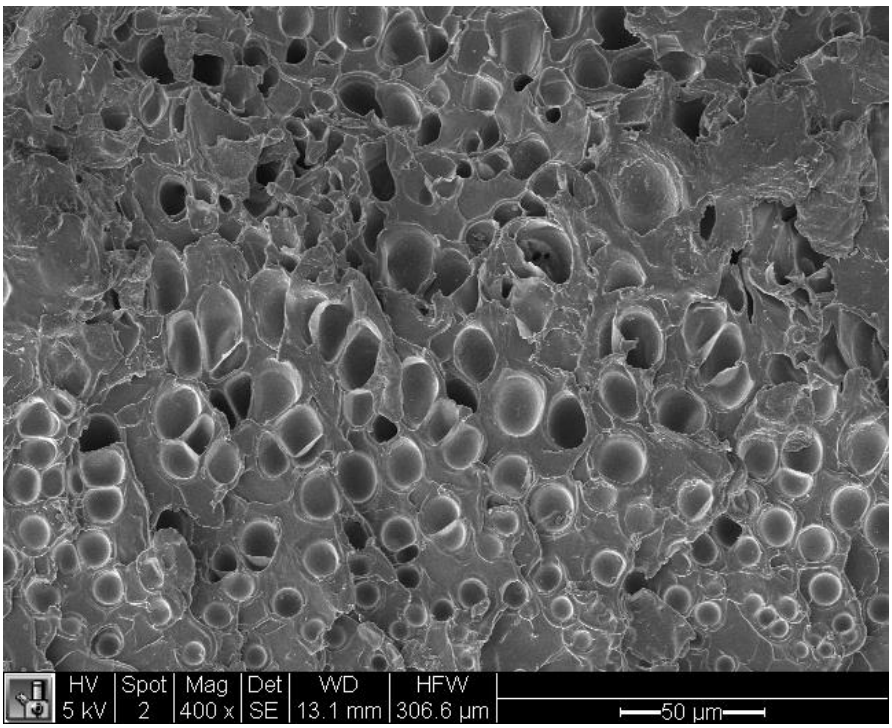

Figure A.29b: These cells appear to have a much more uniform (and circular) shape than the previous SEMs at 1 MPa.

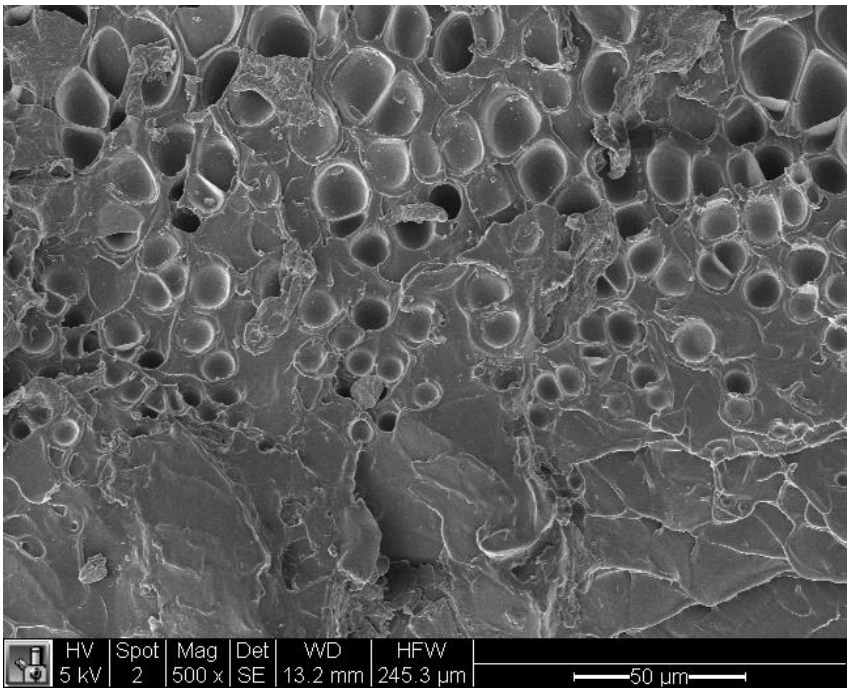

Figure A.29c: A closer look at the transition region of the microstructure. Here the transition appears to be more gradual, as opposed to the stark change in structure for the previous specimens at 1 MPa.

S3 - 7/7 (status: **successfully foamed**):

Speed: 46%, Power: 10%

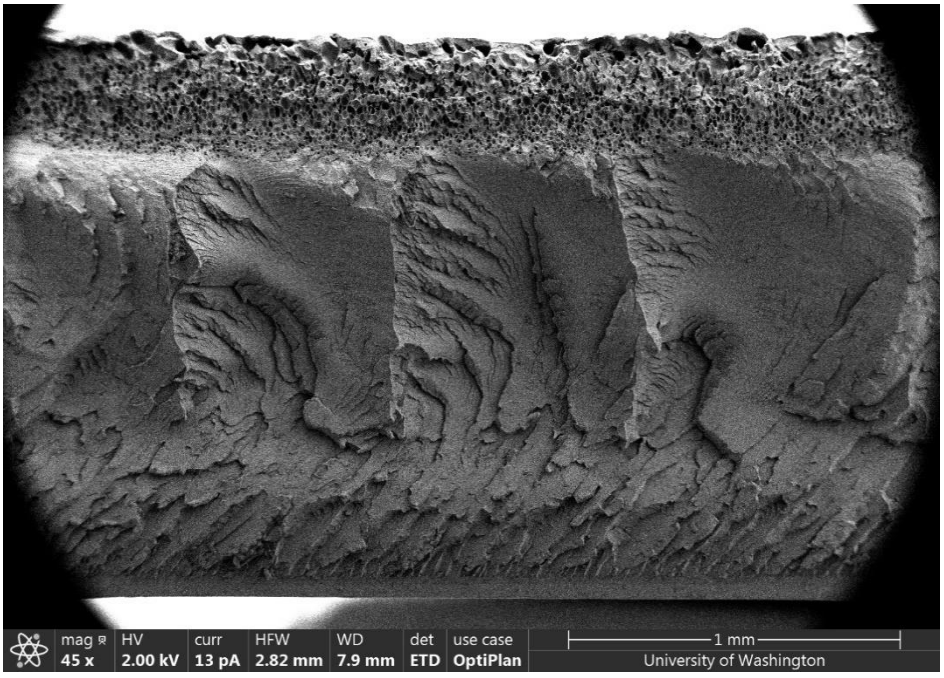

Figure A.30a: Full depth thickness of the specimen. Under the foamed layer, clear evidence of artefacts (fracture marks) can be observed.

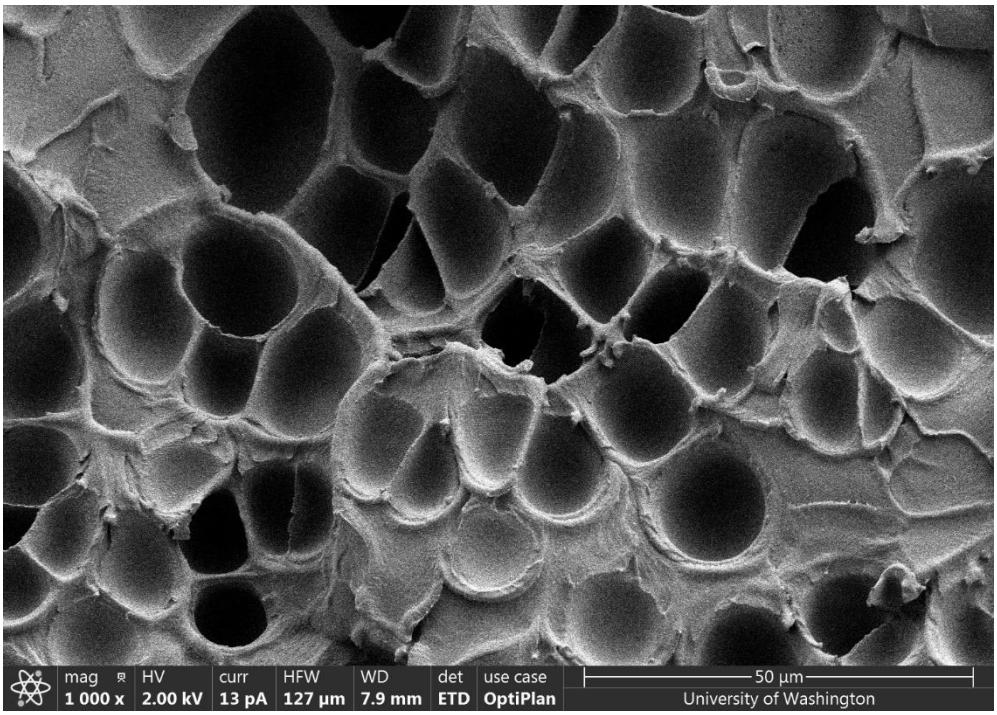

Figure A.30b: A closer look at the bubbles reveals the much larger scales that nucleation brings the final bubble sizes to. The bubble sizes appear to range between 10-15 microns and appear to be very circular.